TÉCNICO LISBOA

Modelling PLN R14del cardiomyopathy using hiPSC-derived cardiac spheroids and organoids

Adriana Silva Passadouro

Thesis to obtain the Master of Science Degree in

Biological Engineering

Supervisors: Prof. Joost P.G. Sluijter
Prof. Cláudia Alexandra Martins Lobato da Silva

Examination Committee

Chairperson: Prof. Maria Margarida Fonseca Rodrigues Diogo
Supervisor: Prof. Joost P.G. Sluijter
Member of the Committee: Dr. Mariana da Mota Veiga de Araújo Branco

November 2021

Preface and Declaration

The work presented in this thesis was performed at the Department of Experimental Cardiology Laboratory, Regenerative Medicine Center Utrecht of UMC Utrecht (Utrecht, the Netherlands) during the period February-July 2021, under the supervision of Prof. Joost Sluijter, within the frame of the Erasmus+ programme. The thesis was co-supervised at Instituto Superior Técnico by Prof. Cláudia Lobato da Silva.

I declare that this document is an original work of my own authorship and that it fulfils all the requirements of the Code of Conduct and Good Practices of the Universidade de Lisboa.

Acknowledgments

This project compiled a whirlwind of emotions that have enriched me at a personal and academic level. There are, fortunately, a lot of people to acknowledge for it.

I have to start by thanking Prof. Joost Sluijter for accepting me as a student so long ago and believing in my potential yet again to pursue this project with an incredible example of both a professional and warm work environment. More specifically, to Renee Maas, there are no proper words to even begin to thank you for everything you have done during this whole time and allowing me to grow as a scientist and a person. I have thanked you for a lot more but this project turned out to be an enriching experience mostly because of you and your supervision. To both Dr. Magdalena Harakalova and Dr. Frank van Steenbeek, your support was incredible and the welcoming environment you created throughout this project allowed me to thrive during this experience. I want to thank Prof. Cláudia Lobato da Silva for an exemplary guidance and incredible support. Your kindness and patience were outstanding and, without it, this really would not have been possible. All of you mentioned above motivated me when most needed as I never felt alone even away from home and had the conditions necessary to perform the best I could.

This also extends to my friends that were always there when things seemed too overwhelming to bear. My group of friends that stuck with me during this year, what I can say is that a ”thank you” is not enough and never will be. All of you Marta Gaspar, Beatriz Sobreira, Luis Lisboa, Rafael Alves, Carlos Clara and Henrique Mamede have unmatched patience and amazing hearts and without even one of you this project would not have happened. Starting with your support since day one in this university and adding the help network you created for me at this final stage, it really is obvious that I am surrounded by amazing human beings that bring out the best in me when I can't.

Para a minha família, a minha mãe, pai e irmão não dá para agradecer o facto de ter sido possível concretizar este trabalho depois do ano que passou. O ambiente que proporcionaram tornou este projeto mais fácil de fazer enquanto se lidava com imensas coisas e inseguranças. Sempre que eu achava que ou não era capaz ou não valia a pena, faziam-me ver o contrário, o que resultou nisto e no incrível final deste processo todo. Para vocês, parte deste trabalho também é muito vosso.

For all of you mentioned above, part of both this project and my achievements are also yours in your own way.

Abstract

Cardiomyopathies are a group of structural and functional disorders of the heart muscle that often lead to heart failure, caused by combined genetic and acquired triggers. Phospholamban (PLN) is a cardiac protein involved in Ca^{2+} homeostasis in cardiomyocytes (CMs), being a crucial regulator of cardiac contractility. Deletion of arginine 14 in the PLN gene (R14del) cardiomyopathy is a severe, not yet fully understood disease. R14del is associated with the dilated cardiomyopathy (DCM) phenotype, including ventricular arrhythmias, cardiac fibrosis and sudden cardiac death, with no effective treatment available. Thus, the current *in vitro* systems available fail to translate, not providing a proper insight into the complex dynamics of the human heart. Alternatively, three dimensional (3D) models can recapitulate the native tissue's microenvironment and its pathophysiological conditions, possibly comprising cells derived from human induced pluripotent stem cells (hiPSCs), obtained from patients with specific known genotypes. Specifically, using R14del patient-specific hiPSC-derived CMs can help bridging the disease modelling gap and elucidate on the link between impaired contractility, Ca^{2+} mishandling and the amount of fibrosis in the hearts of PLN R14del patients.

In this project, a new methodology for the generation of cardiac spheroids was developed and a technique for human cardiac organoids (hCOs) generation was adapted and optimised using mutation carrier and healthy cell lines. The systems established permitted the study of 3D cellular architecture, detection of cardiac fibrotic remodelling in PLN R14del, beating rate measurements and Ca^{2+} transients analysis, where a clear contrast was identified between PLN R14del and control (CTRL).

Keywords

cardiac organoids; cardiac spheroids; cardiomyocytes; PLN R14del; cardiomyopathy.

Resumo

Cardiomiopatias são um grupo de patologias estruturais e funcionais do músculo cardíaco que, frequentemente, provocam paragem cardíaca, causadas por uma combinação de fatores genéticos ou adquiridos. PLN é uma proteína cardíaca envolvida na homeostasia de Ca^{2+} em cardiomiócitos, sendo um regulador crucial da contração. A deleção de arginina 14 no gene PLN (R14del) causa uma doença crítica e não inteiramente entendida. É comparável com DCM, apresentando arritmias ventriculares, fibrose e morte súbita cardíacas, com nenhum tratamento eficaz disponível. Desta forma, é perceptível que os atuais sistemas *in vitro* não possibilitam uma visão adequada sobre a dinâmica complexa do coração humano. Contrariamente, modelos 3D recapitulam o microambiente do tecido e as suas condições patofisiológicas, podendo ser formados por células derivadas de hiPSCs, obtidas de pacientes com um genótipo conhecido. Especificamente, usar cardiomiócitos derivados de hiPSC de pacientes R14del pode ajudar a modelar a doença *in vitro* e esclarecer a ligação entre contração afetada, transporte de Ca^{2+} e a quantidade de fibrose no coração destes pacientes.

Consequentemente, neste projeto, uma nova metodologia para construção de esferoides cardíacos foi desenvolvida e outra para a formação de organoides cardiacos foi adaptada e otimizada, usando linhas celulares saudáveis e de pacientes de PLN R14del. Os sistemas desenvolvidos permitiram um estudo da arquitetura celular em 3D, identificação de remodelação fibrótica em PLN R14del, medida de ritmo cardíaco e análise de transientes de Ca^{2+}, onde um claro contraste entre PLN R14del e CTRL foi identificado.

Palavras Chave

cardiomiócitos; cardiomiopatia; esferoides cardiacos; organoides cardiacos; PLN R14del.

Contents

List of Figures

List of Tables

Acronyms

2D	Two dimensional
3D	three dimensional
AP	action potential
APC	adenomatous polyposis coli
ASC	adult stem cell
ATP	adenosine triphosphate
BMP	bone morphogenic protein
bpm	beats per minute
BSA	bovine serum albumin
cDNA	complementary deoxyribonucleic acid
CF	cardiac fibroblast
CFTR	cystic fibrosis transmembrane conductance regulator
CICR	Ca^{2+}-induced Ca^{2+} release
CK-1	casein kinase-1
CM	cardiomyocyte
CNC	cardiac neural crest
CO	cardiac organoid
COL1A1	collagen type 1
CRISPR	Clustered Regularly Interspaced Short Palindromic Repeats
CTRL	control
CVD	cardiovascular disease
DAPI	4',6-diamidino-2-phenylindole

DCM	dilated cardiomyopathy
DMSO	dimethylsulfoxide
DVL	disheveled
EB	embryoid body
EC	endothelial cell
ECC	excitation-contraction coupling
ECM	extracellular matrix
EDTA	ethylenediaminetetraacetic acid
EHT	engineered heart tissue
ER	endoplasmic reticulum
ESC	embryonic stem cell
FACS	Fluorescence-activated cell sorting
FBS	fetal bovine serum
FGF	fibroblast growth factor
FHF	First Heart Field
GSK3	glycogen synthase kinase 3
KO	Knockout
hADSC	human adipose-derived stem cell
hCO	human cardiac organoid
hECT	human engineered cardiac tissue
HEK	human embryonic kidney
hESC	human embryonic stem cell
HF	heart failure
HFO	heart-forming organoid
hHO	human heart organoid
hiPSC	human induced pluripotent stem cell
hPSC	human pluripotent stem cell
HUVEC	human umbilical vein endothelial cell
ICD	implantable cardioverter defibrillator
IF	immunofluorescence

iPSC induced pluripotent stem cell

ISL1 LIM-homedomain transcription factor Islet1

ISO isoprenaline

LEF lymphoid enhancer-binding factor

LRP5/6 lipoprotein receptor related protein 5/6

LTCC L-type Ca^{2+} channels

MRI magnetic resonance imaging

MSC mesenchymal stem cell

NCX Na^{+}/Ca^{2+} exchanger

PBMC peripheral blood mononuclear cell

PBS phosphate-buffered saline

PCR polymerase chain reaction

PFA paraformaldehyde

PKA protein kinase A

PLN Phospholamban

PORCN porcupine

Pro-COL1A1 Pro-collagen type 1

PSC pluripotent stem cell

RNA ribonucleic acid

ROCK rho-associated coiled-coil protein kinase

RYR2 ryanodine receptor type 2

SERCA2a sarcoplasmic reticulum Ca^{2+}-ATPase pump

SHF Second Heart Field

SR sarcoplasmic reticulum

TCF T-cell factor

VEGF vascular endothelial growth factor

Wnt wingless-type mouse mammary tumour virus integration site

WT wild type

Motivation and Context

cardiovascular diseases (CVDs), including cardiomyopathies, are the number one cause of death globally, according to the World Health Organization [4]. Thus, they have taken centre stage in many biomedical research projects. Genetic predisposition, such as mutations in Phospholamban (PLN), have a relevant causal link in the development of cardiomyopathies. Cardiomyopathies are disorders of the cardiac muscle that cause mechanical and/or electrical dysfunction. Since cardiomyocytes (CMs) are the key component for cardiac contraction which is regulated by Ca^{2+} homeostasis in each CM, it is natural that pathologies linked to a disruption in the beat-to-beat controlled Ca^{2+} handling process amount to a third of all deaths in the developed world [5].

PLN is a 52-amino acid protein located in the sarcoplasmic reticulum (SR) membrane that acts as a reversible regulator of Ca^{2+} uptake in the CM [6]. PLN R14del is a mutation linked to an impaired Ca^{2+} reuptake and contractility resulting in malignant arrhythmias and sudden cardiac death [6, 7]. This mutation presents a highly variable phenotype, which ranges from asymptomatic to cardiomyopathic, and its awareness is rather low, therefore, thousands of people can be carriers unknowingly [7]. This also means that once diagnosed, it can be too late for some to get medical treatment. The Netherlands currently has the largest PLN cardiomyopathy patient population (in 2020 alone, more than 1500 people were diagnosed with the mutation in The Netherlands and thousands still unidentified). Additional families carrying the PLN R14del mutation have been recognized in other European countries, the United States, and Canada [8, 9].

To raise awareness on the mutation carriers' phenotype, more efficiently identify carriers and possibly develop new therapies, it is key to have a better understanding of the pathological mechanisms. It remains unclear how exactly the PLN R14del mutation leads to such severe cardiomyopathy and malignant arrhythmia [10]. Cardiovascular biology researchers and pharmaceutical industries have long relied on cell culture and small animals screenings which, however upgraded they have been over the years using immortalized cell lines or more complex animals, still pose a major issue due to their low disease relevance and poor *in vivo* recapitulation of human physiology [11].

human induced pluripotent stem cell (hiPSC) technology has constituted a significant tool in the field without the ethical constraints typically associated with human research, bridging the technological and

knowledge gap associated with commonly used models. The generation of more physiological cardiac models, new assay formats and innovative and more robust screening technologies have been developed, better recapitulating human *in vivo* physiology in order to improve upon translational applications since hiPSCs can be patient-derived [12, 13].

Two dimensional (2D) models often lack in accurate organ modelling, disregarding several cell types and tissue organization. A proper insight into the complex dynamics of the human heart could be better obtained using a three dimensional (3D) model taking into consideration both cell-cell and cell-extracellular matrix (ECM) dynamics and tissue dynamics between each cell layer. Importantly, attempts have been recently made to produce more complex, multicell-type 3D heart tissues or organoids. Tissue engineering approaches, while allowing for high control of the end construct, are expensive, work intensive and in most cases not readily scalable or easy to implement. Fortunately, the last decade has seen the emergence of organoid-based approaches which are self-assembling 3D cell constructs composed of significant organ-specific cell types and can recapitulate organ-specific functionality and structure to a significant extent. Such models can make up for a more physiological, efficient and reproducible model that can allow for a better understanding of pathological phenotypes and, consequently, the correct identification of potential drug targets and their safety issues in a robust manner [14, 15].

Reasonably, a 3D organoid hiPSC model would be ideal for a better characterization of PLN R14del cardiomyopathy to circumvent shortcomings associated to previously developed models. As administration of standard heart failure (HF) therapy does not rescue the mutation's phenotype, there is no specific therapeutic treatment for PLN-R14del-related cardiomyopathy. This undoubtedly highlights the pressing demand for better representation of the pathology and evaluation of new treatment assays to slow down or even reverse the severe phenotype [6].

1

Introduction

Contents

1.1 PLN R14del-related cardiomyopathy

The heart's uninterrupted function from embryogenesis throughout adulthood is the basis for life in all animals. Understandably, factors as abnormal embryogenesis leading to congenital heart diseases, acquired malfunctions and inherent genomic mutations can be linked to abnormal and pathological function with fatal consequences, putting CVDs in the lead for the most deadly condition in the western world [4]. Furthermore, this organ has a very limited potential for regeneration and repair, being unable to generate new cardiac muscle upon significant loss, which results in eventual ischemic episodes and even heart failure [16].

Events leading to heart failure are mostly related to CMs deficiency. CMs show high-level expression of genes that encode contractile force-generating sarcomere proteins and calcium-mediated processes (ryanodine receptor type 2 (RYR2) and PLN) [17]. Provided that the trigger for cardiac contraction is the elevation of the Ca^{2+} concentration in the cytoplasm of the CM, any mutation in the PLN gene, tightly connected to the function of a Ca^{2+} pump, is naturally critical to calcium homeostasis, giving rise to cardiomyopathy. To unravel pathological molecular mechanisms, potentially identify symptoms at an earlier stage or develop innovative screening technologies for effective drugs, the cardiovascular research community still faces considerable challenges. The complexity of the heart, diverse cellular population along with its organization, signalling pathways and regulatory networks of cardiac development remain as the paramount challenges [16].

1.1.1 Cardiac embryonic development

Cardiogenesis refers to the series of events that make up the development of the embryonic heart. It is a complex process to describe and study as it involves a functional synchrony between a diverse population of cells as presented in Figure 1.1. The process is precisely regulated by signalling pathways and networks of transcription factors, which are spatially and temporally controlled in each developmental stage [16, 18]. The heart is the first functional organ in the embryo and is said to be morphologically complete by 8 weeks of gestation in humans [19]. The complexity of the molecular cascades in cardiogenesis is also highly correlated with the heart's sensitivity to either embryonic or age-related anomalies [20].

Firstly, bone morphogenic protein (BMP) is secreted by the endoderm and modulates CM fate, while wingless-type mouse mammary tumour virus integration site (Wnt)-mediated signals from the neural tube inhibit cardiac specification [16]. Two progenitor cell types assemble on either side of the midline where the first heart progenitors differentiate and localize in the anterior mesoderm composing what is called the First Heart Field (FHF) in the cardiac crescent stage [16]. In an anterior position to the cardiac crescent, the Second Heart Field (SHF) is formed also from a mesodermal origin where progenitor cells

receive inhibitory Wnt signals and remain in an undifferentiated state for longer, distinctively identified by the expression of the *LIM-homedomain transcription factor Islet1 (ISL1)*. The first beating structure is later formed by the linear heart tube (E20). Consecutively, the interaction between FHF and SHF progenitors contributes to heart tube elongation, looping, ballooning and septation, originating the four-chambered structure typical of an adult heart. FHF and SHF both are highly involved in the formation of the left and right ventricles, respectively [16, 19, 21]. The heart's maturation stage entails septation of either ventricles and atria along with valve formation by E32, being fully functional at birth [16, 21].

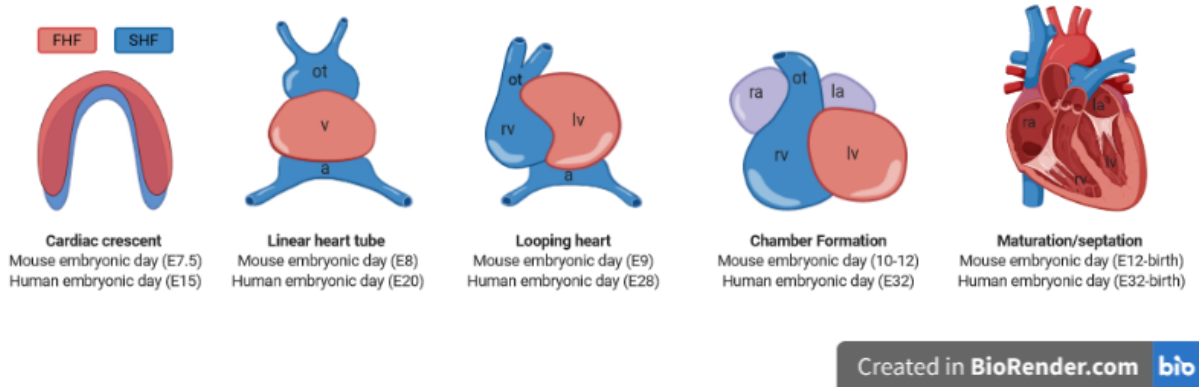

Figure 1.1: Developmental stages and embryonic structures of cardiogenesis along mouse and human embryogenesis [16, 21]. **FHF**- First Heart Field, **SHF**- Second Heart Field, **ot**- outflow tract, **v**- ventricle, **a**- atria, **rv**- right ventricle, **lv**- left ventricle, **ra**- right atrium, **la**- left atrium. Created with Biorender.com.

At day 22 after fertilization, the primitive human heart starts to beat in the absence of external cues. Reaching day 50, during the fifth week, neural crest cells migrate, aggregate and differentiate, potentiating rich parasympathetic innervation prior to the sympathetic one. Cardiac autonomic nerves significantly innervate and highly influence atrial and ventricular CMs regulating their contraction force (inotropy) and relaxation (lusitropy). Along the maturation process, the sympathetic and parasympathetic cardiac nervous system also modulates heart rate (chronotropy) and the velocity of electrical impulses in the heart (dromotropy) [22]. Factors such as the interaction between intrinsic and extrinsic signals, the crosstalk between molecules in the FHF and SHF and ultimately the regulation by cardiac neural crest (CNC) cells makes cardiogenesis notably more complex to recapitulate *in vitro*, given that the FHF, SHF and CNC are originated in very distinct embryonic germ layers (mesoderm and ectoderm) [16, 18, 23]. In addition, the course of cardiac differentiation, specification and overall development due to the activation or repression of a myriad of signalling pathways contribute to the distinct molecular and functional profiles of cardiac cells, which are both crucial for their diverse physiological roles in the heart.

1.1.2 Human Cardiac Physiology

Understanding the complex mammalian heart's structure, diverse cellular population and organisation is then key to develop novel therapies. Structurally, the mammalian heart is divided into four chambers - the right and left atria and the right and left ventricles - and the human heart's wall is organized in three layers: endocardium (smooth muscle and elastic fibers), myocardium (cardiac muscle) and epicardium (connective and adipose tissue) [24].

The endocardium is formed by endocardial cells, which are specialized endothelial cells (ECs) that constitute the interior lining of blood vessels and cardiac valves. Through genetic lineage–tracing technology, endocardial cells have been reported to be able to originate different cardiac cell types during embryonic development, which highlights the endocardium's plasticity and points to an unexpected role of the endocardium in heart regeneration [25].

The epicardium is a thin mesothelial tissue comprising the outermost layer of the heart in vertebrates and consists of a heterogeneous population of epicardial cells which give rise to the precursors of the coronary vasculature and cardiac fibroblasts (CFs) [26]. The epicardium has also been reported to play a crucial role in not only the heart's embryonic development but also in repair upon injury as there is mounting evidence on epicardial cells' high plasticity upon activation [27]. Once activated, this outer layer can interact with the myocardium, with the stimulation of several signalling pathways and promote CM proliferation along with maintaining both cardiac tissue structure and CMs' electrophysiological properties [27].

The myocardium is responsible for muscle contraction and it is made up of three different cell types including atrial and ventricular CMs, CFs and ECs [28]. The myocardium is considered a post-mitotic tissue with little to no regenerative capacity as it is mainly constituted of CMs which are believed to not re-enter the cell cycle, after embryogenesis [16]. Atrial and ventricular myocytes make up 30% of the heart and CFs represent about 60%. The remaining 10% include pacemaker cells, ECs, epicardial cells and pericytes [1]. CFs produce the connective and elastic ECM, being responsible for myocardial tissue structure maintenance and remodelling, whereas endothelial cells constitute the vasculature and supply nutrients to the cardiac cells, regulating the contractile state of CMs through autocrine and paracrine signalling molecules [29]. CMs, which make up one third of the heart, are the fundamental unit responsible for conduction of electrical impulses and contraction of the cardiac muscle [19]. Other cell types such as pacemaker cells and Purkinje fibres present in the conduction system are specialized CMs that initiate and control electrical impulses [16]. Pacemaker cells are responsible for initiating each cycle of cardiac muscle activity, setting the pace and rhythm of the heart beat. As these cells are later supported by the Purkinje network which ensures the spread of the electrical impulse to the muscular ventricular walls, both promote contraction of the heart as a pump [16]. In addition, both cell types contribute to CMs' differentiation, proliferation and function as heart muscle contraction and relaxation comprehends

a highly coordinated process [19]. In Figure 1.2, the diverse cellular population in the four-chambered heart is represented along with their localization.

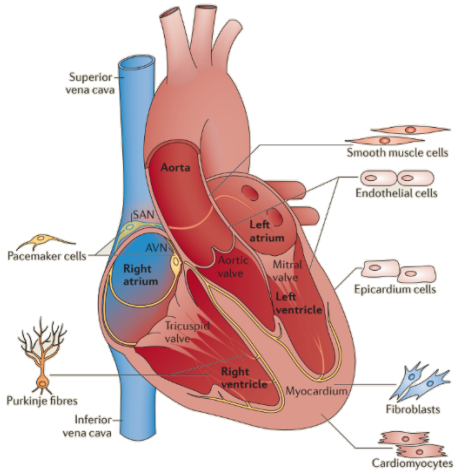

Figure 1.2: Schematic representation of the heart's cell types and structural organisation. Adapted from reference [16].

The pump function of the heart is mediated by the synchronous contraction of the CMs where intracellular Ca^{2+} handling is a tightly-controlled process to ensure optimal electrical and mechanical CM function. excitation-contraction coupling (ECC) is the process in which the action potential (AP) generated by pacemaker cells is transducted into the CMs' contractile response and is illustrated in Figure 1.3.

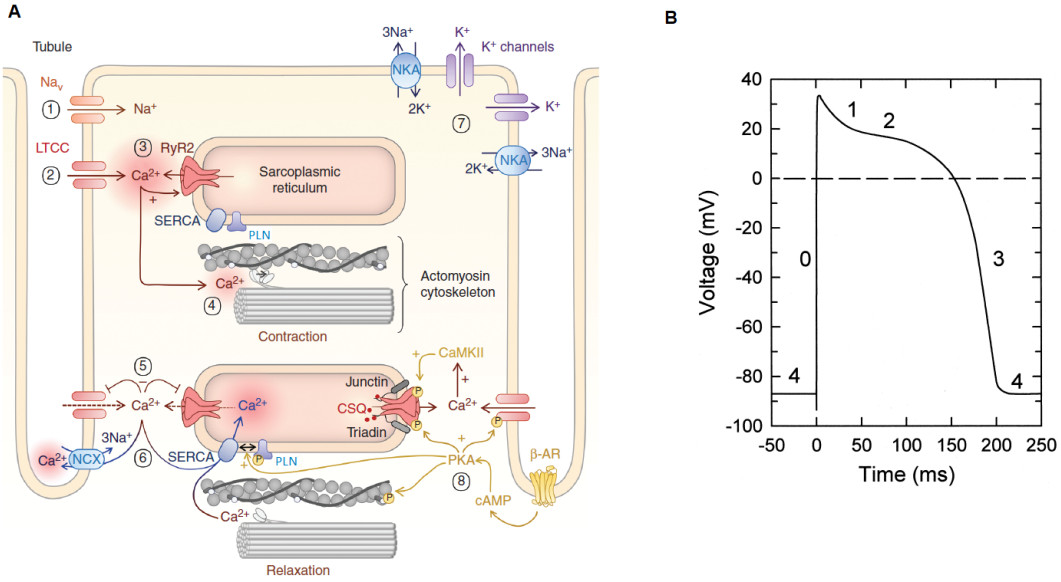

Figure 1.3: **A**: Schematic representation of ECC (the numbered events in ECC are depicting each step in cardiac contraction and relaxation) [5]; **B**: ventricular action potential. The five phases of the ventricular AP are labeled [30].

During systole, a transient depolarization of the CM plasma membrane (sarcolemma) is induced as voltage-dependent Na^+ channels open (**step 1**). This causes an inward current of Na^+ triggering a Ca^{2+} influx through voltage-dependent L-type Ca^{2+} channels (LTCC) (**step 2**). These channels potentiate an increase in intracellular Ca^{2+} when activated protein kinase A (PKA) phosphorylates them. This Ca^{2+} influx is not by itself sufficient to induce effective mechanical contraction. However, Ca^{2+} entering the cell stimulates the opening of RYR2 channels located on the SR through a mechanism called Ca^{2+}-induced Ca^{2+} release (CICR) (**step 3**). As these channels open, Ca^{2+} is also significantly released from the SR to the cytosol. As Ca^{2+} diffuses throughout the cytosol, the high cytosolic Ca^{2+} concentration promotes Ca^{2+} binding to troponin-C, part of the myosin filament of the sarcomere, which exposes the actin binding sites (**step 4**). This way, the formation of crossbridges is possible resulting in force generation that translates into CMs contraction [5, 31–33].

Diastole (heart's relaxation) occurs with the unbinding of Ca^{2+} from troponin-C enabling its connection to actin which blocks the myosin binding site. LTCC are innactivated, RYR2 closes and relaxation proceeds (**step 5**). Cytosolic Ca^{2+} is reuptaken by the SR through the sarcoplasmic reticulum Ca^{2+}-ATPase pump (SERCA2a) pump. SERCA2a is mediated by PLN and the SR is the major source of contractile Ca^{2+} in adult mammalian hearts, needing Ca^{2+} restorage for subsequent release [30]. Simultaneously, the Na^+/Ca^{2+} exchanger (NCX) removes it from the cell, decreasing cytosolic Ca^{2+} concentration (**step 6**). Finally, before a new cycle starts, the membrane potential restores its resting value as cell repolarization with K^+ efflux takes place (**step 7**) [5, 31–33]. Interestingly, while the heart adapts to cardiovascular demands, PKA phosphorylation of LTCC can occur due to the activation of the β-adrenergic signalling pathway involving β_1 and β_2 adrenergic receptors (**step 8**) [34]. Naturally, elevated concentrations of intracellular Ca^{2+} increase inotropy in the heart, which can be stimulated by several cardioactive compounds. Isoproterenol is a non-selective β adrenergic receptor agonist which activates the β-adrenoceptor subtypes expressed in CMs (β_1 and β_2), presenting cardiac stimulating properties as it increases heart rate in humans [34]. This positive inotrope is commonly known to increase heart rate and ventricular oxygen consumption thus enhancing contractility and is generally used in heart failure or cardiogenic shock [35].

Furthermore, the electrical stimulus inducing CM contraction can be seen in Figure 1.3 **B**. Understanding the electrophysiological characteristics of the cardiac AP is pivotal towards unraveling cardiac disease mechanisms associated with Ca^{2+} mishandling. "Phase 0" is termed the "rapid upstroke phase" when Na^+ channels are activated and depolarization of the membrane potential occurs as it shifts into positive voltage range (**step 1**). "Phase 1" is the relatively brief repolarization phase that immediately follows the upstroke of the AP. This is due to a rapidly turned on transient outward current, where the efflux of K^+ appears as the key current. "Phase 2" is called the plateau phase and it is the longest one, marking the phase of prolonged inward flow of Ca^{2+} into the cell (**step 2**), which is enhanced by

Ca^{2+} release from the SR Ca^{2+} store (CICR) (**step 3**). "Phase 3" is the late or final repolarization phase following the AP plateau. It takes place upon the inactivation of the LTCC, when the delayed and inward rectifier K^+ channels are activated, creating an outward current, resulting in the repolarization of the cell (**step 7**). "Phase 4" is the resting potential, when the AP ends and is stable at ~ -90 mV in normal working myocardial cells. Naturally, dysregulation of any of these transport mechanisms will lead to a new cardiac adaptation, possibly with a new AP configuration and cardiac output [5, 30, 36].

1.1.2.A PLN R14del pathological Phenotype

Cardiac development and pathology are regulated by Ca^{2+} signalling pathways acting on gene expression and CM growth, also being crucial for Ca^{2+} homeostasis in the heart. Interestingly, altered Ca^{2+} underlies a number of pathological events such as inappropriate cardiac growth, rhythmic disturbances and heart failure [5]. Specifically, CM dysfunction and consequent arrhythmias can arise from an increase in cytosolic Ca^{2+} concentration or prolonged intervals of increased Ca^{2+} [37].

Hence SERCA2a's pump function to reuptake Ca^{2+} into the SR is critical to prevent functional abnormalities. SERCA2a is partially regulated by PLN, a small 52 amino acid membrane-associated protein, which can reduce SERCA2a's affinity to Ca^{2+}. The inhibition of SERCA2a prevents the influx of Ca^{2+} to the SR and prolongs the increase in cytosolic Ca^{2+}. When PKA phosphorylates PLN, its inhibitory effect is reduced and SERCA2a is activated, increasing the Ca^{2+} flux into the SR. Ca^{2+} cytosolic concentration returns to its resting levels during diastole [31]. Evidently, mutations in the PLN gene are highly linked to the disruption of the SERCA-induced balance of Ca^{2+} handling.

The deletion of arginine 14 codon (R14del) in the PLN gene has an irreversible super-inhibition effect of SERCA2a activity, resulting in blockage of Ca^{2+} reuptake [38]. PLN R14del-related cardiomyopathy can be characterized by early onset and the presence of lethal ventricular arrhythmias and was first described in a large Greek family [7, 39]. Several dominant mutations in PLN have been associated with dilated cardiomyopathy (DCM), including the R14del mutation that is a founder mutation in the Netherlands and Germany. Interestingly, the R14del mutation appeared to be the most prevalent cardiomyopathy-related mutation in the Netherlands, being present in 15% of patients with DCM [7].

DCM is inherited commonly as a dominant disorder associated with a range of genetic defects where abnormal Ca^{2+} handling is present as a hallmark of the disease's phenotype. [37, 38, 40]. Arising from a variety of genetic and acquired triggers, the clinical course of patients with DCM is remarkably heterogeneous given distinct pathophysiological features [41]. Remarkably, DCM is characterized by substantial myocardial fibrosis up to 36% of total left ventricle mass with a midwall distribution throughout the left ventricle, which is a feature correlated to disease severity [42]. When compared to other mutation carriers, patients with a PLN mutation have a higher frequency of left ventricle structural and functional abnormalities and they show the most pronounced diminished left ventricle function detected

by echocardiography and cardiac magnetic resonance imaging (MRI) [7]. Moreover, PLN R14del hearts were compared with hearts with desmosomal, lamin A/C, sarcomeric and desmin mutations and presented the highest amount of myocardial fibrosis which is found in a distinct pattern in the posterolateral left ventricle wall (Figure 1.4**C**) [42]. Ultimately, it has been determined that PLN R14del mutation carriers have higher incidence of malignant ventricular arrhythmias with left ventricular ejection fraction <45%, premature sudden cardiac death and end-stage heart failure when compared to DCM patients that do not carry this pathogenic variant [6, 38].

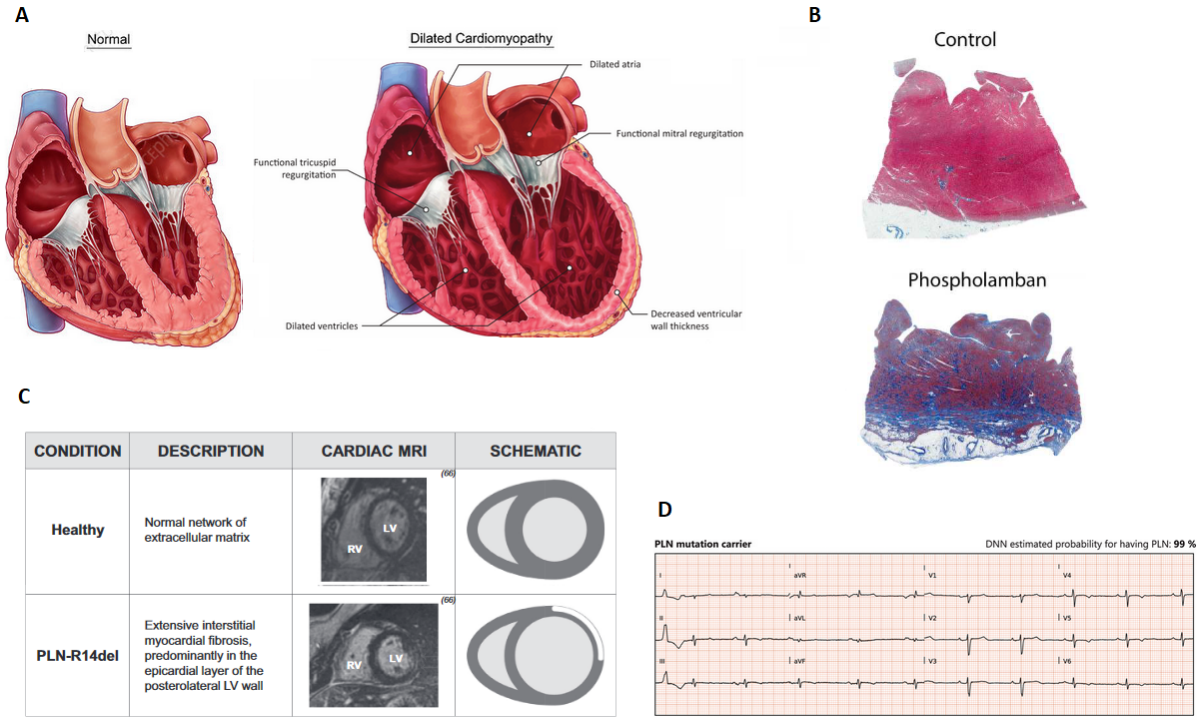

Figure 1.4: Overview of PLN R14del related cardiomyopathy phenotype features. **A**: Characteristic alterations in cardiac morphology underlying heart failure in DCM [43]; **B**: Masson's trichrome stains of the myocardium of the left ventricle of a control and a PLN R14del heart (Fibrosis is stained in blue, CMs in red and adipocytes in white) [44]; **C**: Distinct type and pattern of myocardial fibrosis associated with PLN R14del. Healthy myocardium is visualized as dark areas without fibrosis, while fibrotic patches are observed as bright areas [42]; **D**: Representative example of an electrocardiogram of a PLN mutation carrier (DNN: deep neural network probability score for having the PLN mutation) [45].

1.1.3 PLN R14del *in vitro* models

Given the highly variable phenotype of patients with PLN R14del-related cardiomyopathy, ranging from asymptomatic to cardiomyopathic, the prognosis is significantly poor. Therefore, it is understandable that the assessment of the molecular mechanisms underlying the pathogenesis of the disease becomes an even more difficult task [7].

Nevertheless, in the past decade, research using animal models has provided insights into the genetics and physiology of the heart. Complemented by work with cellular models using human pluripotent stem cells (hPSCs), including human embryonic stem cell (hESC) and hiPSC, the field is progressing with providing proper insight into the complex dynamics of the human heart as a whole. In Table 1.1, a comprehensive summary of the existing PLN R14del-related cardiomyopathy models is depicted along with their specifications and outputs.

Table 1.1: Summary of the different types of PLN R14del models, along with their specifications and outputs.

Model	Methods	Year of introduction	Cell type	Readout	Reference
mouse	human embryonic kidney (HEK)-293 were transfected with complementary deoxyribonucleic acids (cDNAs) encoding wild type (WT)-PLN and PLN-R14Del in expression constructs. The site-specific R14 deletion was introduced into mouse PLN cDNA by polymerase chain reaction (PCR).	2006	HEK-293 Mouse	Coexpression of the normal and mutant-PLN in HEK-293 cells resulted in SERCA2a super-inhibition. Super inhibitory effect was diminished by PKA, although not fully relieved. Mutant PLN-R14del mice presented a significant increase in heart size. Histological analysis of transgenic mice revealed ventricular dilation, myocyte disarray, and myocardial fibrosis. A Ca^2+ uptake assay confirmed super inhibition of the Ca^2+ affinity for SERCA2a, resulting in premature death of transgenic mice.	[39]
hiPSC-CMs	hiPSC-CMs derived using a direct differentiation method maintained in basal differentiation media for up to 4 weeks. Ca^2+ transient analysis: performed 30-days post differentiation, upon loading a fluorescent Ca^2+ sensitive dye, Fura-2.	2015	hiPSCs	Arrhythmic Ca^2+ cycling profile generated (higher spontaneous beating rate and frequent episodes of irregular Ca^2+ waves. Abnormal cytoplasmic PLN protein distribution in CMs detected.	[38]
hECT	Directed differentiation of hiPSC-CMs to generate healthy CMs, PLN R14del-CMs and TALEN-edited isogenic corrected CMs. After 15 days of differentiation, hiPSC-CMs were harvested and mixed with collagen type-I and Matrigel solution. The cell-matrix suspension was transferred into polydimethylsiloxane (PDMS) moulds, with integrated cantilever end-posts.	2016	hiPSCs	PLN R14del mutation impaired cardiac contractility and genetic correction restored contractile function. In mutant human engineered cardiac tissues (hECTs), the intracellular distribution of PLN within CMs was polarized at one side of the cell.	[46]
mouse	Mice carrying the PLN R14del pathogenic variant were generated by introducing an additional PLN exon-3 containing the R14del pathogenic variant. Cre-loxP-mediated recombination was used to replace the WT PLN exon-3 with the mutant PLN exon-3.	2020	C57Bl6/N mouse line	Ventricular dilation and contractile dysfunction were reported (left ventricular end-diastolic and end-systolic volumes were increased and stroke volume and ejection faction were decreased as compared to WT controls. Extensive myocardial fibrosis was present throughout the left and right ventricles where fibrotic gene expression levels were also elevated and PLN protein aggregation was detected.	[6]

The previously described models have highlighted a few pathological features linked to PLN R14del cardiomyopathy, unraveling specific phenotypic behaviours. Some of this data has even been correlated to the human disease phenotype. However, further elucidation is still needed to connect the phenotype to disease development and severity. Additionally, it is widely agreed upon that several aspects of the disease still remain unclear, regarding the arrhythmic phenotype and cardiac fibrotic remodelling. Standard cell culture models could fail to bridge this gap when several readouts cannot be performed in an appropriate time point. The use of animal models also does not constitute faithful models, not being representative of human physiology.

1.1.4 PLN R14del available therapies

Cellular models have provided opportunities to study cardiac differentiation and disease *in vitro*. Symptoms develop most often in the fifth decade with a mean age at presentation ranging from 40 to 48 years. However, sudden cardiac death may occur earlier in life and has been reported in patients younger than

30 years old as the onset of the disease appears to be age-dependent with a slightly higher frequency in males [7].

Currently, there are no clinical studies regarding the treatment of patients with a PLN mutation. Withal, it is highly recommended that the current guidelines on heart failure and prevention of sudden cardiac death be applied to determine the optimal medical treatment, exercise restriction, and whether ventricular tachycardia ablation or implantable cardioverter defibrillator (ICD) implantation is indicated [7]. Furthermore, DCM patients with a PLN mutation can exhibit ventricular arrhythmias and experience appropriate ICD therapy more often than DCM patients without a PLN mutation. Even so, patients with genetic mutations are expected to respond less well to treatment as the cause is irreversible, for example when compared with DCM patients with reversible causes, such as viral infection or inflammation [47].

No specific therapeutic treatment options for PLN R14del cardiomyopathy have been identified to date and therefore the current guidelines for heart failure and ventricular arrhythmias are followed. Moreover, standard heart failure therapy does not prevent disease development or increase survival in a previously developed mouse model [6]. Unfortunately, no effective treatment is currently available for PLN R14del patients and the therapeutic option for this cardiomyopathy is heart transplantation which is not a lifetime solution as the average lifespan of a heart transplant is 9.16 years [48]. In 2021, the results of the PHOspholamban RElated CArdiomyopathy STudy - Intervention (i-PHORECAST; ClinicalTrials.gov NCT01857856) are expected. Since myocardial fibrosis is considered to be an early disease manifestation, the i-PHORECAST study aims to test the efficacy of the mineralocorticoid receptor antagonist eplerenone, previously linked to wield antifibrotic effects, in attenuating disease progression or postponing onset of apparent disease in asymptomatic mutation carriers [6, 7].

As studies in human mutation carriers are laborious, expensive and strikingly long, there is an urgent need for efficient, physiological, robust and reproducible disease models. In addition, human CMs are significantly distinct from widely used small animal models such as rodent CMs, namely in their electrophysiological properties, with the mouse heart beating at approximately 500 beats per minute (bpm) and the human heart beating at 60-90 bpm [1]. Human induced pluripotent stem cell (iPSC) technology has been a key tool to innovate the development of novel and more physiological cardiac models to bridge what is lacking in commonly used models. This way, the field is progressing towards recapitulating complex cardiac disorders and to engineer 3D models of the heart *in vitro*.

1.2 hiPSCs and cardiac differentiation

An ideal cell-based disease model would allow for a long-term evaluation of cardiac function, in a controlled laboratory setting, which has proven to be a real challenge in the scientific community. Recent advances in stem cell biology and tissue engineering have provided unprecedented access to human

heart tissue for basic biological studies, disease modelling, drug screening and regenerative medicine applications [49]. Namely, iPSC technology has emerged and proven itself as an extremely valuable tool in drug screenings and disease modelling systems since its discovery in 2006 [50].

hiPSCs are normal primary cells with a stable genotype compared with transformed cell lines and they possess an intrinsic capacity for self-renewal, facilitating their propagation and expansion to constitute drug screening platforms [11]. hiPSCs can also be reprogrammed into many different tissue-specific cell types and they can be derived from any patient in unlimited quantities, allowing for the generation of specific cell types/ tissues that are more difficult to obtain directly from living patients given their invasiveness level, such as neurons, cardiac and pancreatic cell types [51]. More specifically, hiPSCs can be an unlimited supply of cells obtained from patients with known genetic diseases, better representing their pathophysiological phenotypes hence constituting a clinically-relevant platform for cardio-active drugs screening [52].

Deriving CMs from hiPSCs can be efficiently done through defined small molecule differentiation protocols using chemically defined serum free media, which were reported to have reduced lot-to-lot variability of CMs [53–55]. Nevertheless, variability through different cell lines and experimental repeats has resulted in different yields and purity of the obtained CMs, even when identical and fully defined protocols are followed [56]. Reasons underlying cell line related shortcomings have been suggested such as differences in the initial pluripotency state, conditions in which the cell lines are maintained, epigenetic status inherent to the tissue of origin and intrinsic differences in endogenous growth factor production between individual lines [56]. Small molecule-based protocols also deal with the instability and rate of degradation of some growth factors and lot-to-lot variability in their bioactivity, which can affect cell fate outcomes in each lot [56]. Even so, using hiPSCs means there is an unlimited supply and ease of accessibility as compared to native human CMs [52].

Based on the molecular and genetic factors that control CM proliferation and differentiation during early cardiac development, recent differentiation protocols have been developed [57, 58]. The Wnt signalling pathway has emerged as one of the key regulators of cardiogenesis *in vivo* and *in vitro*, presenting an important biphasic role (being turned off and on throughout development) in embryonic cardiac specification, cardiovascular progenitor expansion and CM proliferation (briefly mentioned in section 1.1.1) [59].

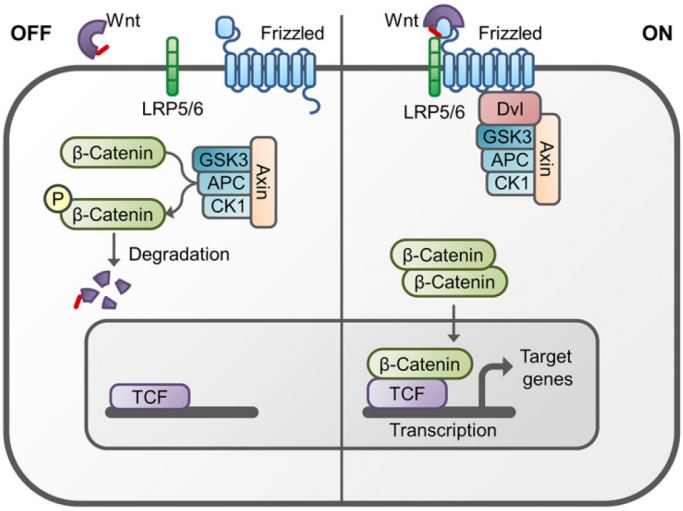

Figure 1.5: Schematic representation of the Wnt/β-catenin signalling pathway according to the state of activation. Adapted from reference [60].

Wnt signalling involves multiple complex signalling cascades (Figure 1.5). In the "off" state, β-catenin is bound in a complex containing glycogen synthase kinase 3 (GSK3)β, and other enzymes (axin, adenomatous polyposis coli (APC) and casein kinase-1 (CK-1)). The kinases in this complex phosphorylate β-catenin, thereby targeting it for degradation by the ubiquitin proteasome system. As for the "on" state, the receptor complex consisting of frizzled and lipoprotein receptor related protein 5/6 (LRP5/6) bound to Wnt ligand recruits the disheveled (DVL) protein to the plasma membrane. This causes the disruption of the β-catenin complex, preventing the phosphorylation of β-catenin. Therefore, this protein becomes stabilized, accumulating in the cytoplasm and translocates to the nucleus to associate with transcription factors and stimulate the transcription of Wnt target genes. In the nucleus, β-catenin binds to T-cell factor (TCF)/lymphoid enhancer-binding factor (LEF) transcription factors, displacing co-repressors and recruiting additional co-activators to activate Wnt target genes transcription [59, 61, 62]. Ultimately, Wnt proteins regulate processes such as proliferation, migration, and differentiation during embryonic development and, at a later stage, in humans, they are intrinsically involved in cardiovascular development [60]. In Figure 1.5, this pathway can be visualized and further understood.

As mentioned, at the level of cytoplasmic degradation of β-catenin, inhibition of GSK3 responsible for β-catenin phosphorylation, results in activation of Wnt signalling. Targeting the isoform GSK3β has also been associated with preserved cardiac function [59]. Cardiac differentiation protocols have then used CHIR99021, a canonical Wnt pathway activator (via specific GSK3β inhibition) [57, 58]. This is directly related to the inhibition of the phosphorylation-mediated β-catenin protein degradation and the stabilization and nuclear accumulation of β-catenin [58–60]. Consequently, β-catenin undergoes nuclear translocation and transactivates Wnt target genes.

Additionally, given the biphasic behaviour feature of the pathway, its inhibition is possible using a

small-molecule Wnt inhibitor, Wnt-C59 (C59) via porcupine (PORCN) inhibition. PORCN is an enzyme in the endoplasmic reticulum (ER) responsible for adding the palmitoleate group to Wnt proteins, and the addition of a hydrophobic group may help to concentrate active Wnt proteins at the cell membrane, which may assist in activation of signalling and induce their secretion [60]. Therefore, PORCN inhibitors block the secretion of Wnt ligands and all PORCN isoforms that can activate the β-catenin-dependent pathway were reported to be substantially inhibited by C59 with dramatic inhibition of endogenous Wnt production [60]. At last, insulin and insulin-free media have been added to the generation of cardiac differentiation protocols with temporal modulation as it inhibits mesoderm formation in favor of ectoderm [63], while protecting cells from apoptosis and stimulating proliferation [56, 57, 64].

Upon cardiac differentiation, the model developed needs to be evaluated for its fundamental characteristics. Taking into consideration either cell-cell and cell-ECM dynamics in the human heart or tissue dynamics between the different cardiac cell layers, there is a high demand for the development of new experimental models that allow for a long-term evaluation of cardiac function in a controlled laboratory setting. Animal models are the most physiological model but there is an imprecise control of complex integrated processes *in vivo* which can mask key underlying mechanisms and present contradictory outcomes. 2D cell cultures on engineered substrates are undoubtedly easier to control than animal models but strikingly non-physiological and present a limited predictability [1, 65]. Instead, 3D systems can provide a microenvironment mimicking the native tissue dynamics and their pathophysiological conditions. This investigation can rarely be performed directly in the organ due to ethical issues and source scarcity. As a result, 3D structures formed by stem cells and consisting of organ-specific cell types have been developed, called organoids.

1.3 Organoid technology

Organoids are defined as 3D structures, mimicking tissue and organ dynamics and structure. They are composed of organ progenitors or different stem cell types typically present in the organ it intends to resemble with the ability to self-organize through cell sorting and spatially restricted lineage commitment, reflecting organogenesis *in vitro* [66]. These structures are expected to present both functional similarities and homologous gene expression profiles compared to their *in vivo* tissue counterpart [67].

Organoids can be derived from pluripotent stem cells (PSCs) either embryonic or induced, and from organ-specific adult stem cells (ASCs), which are tissue-specific resident stem cells. ASCs have been receiving more attention recently for their intrinsic abilities to self-renew and differentiate into the cell types from their respective adult tissues, being therefore essential for mature organ homeostasis and regeneration. These tissue mechanisms occur *in vivo* while the cells maintain genomic stability, which is strikingly advantageous for the formulation of an organoid structure [68].

The starting point for many organoid models is an embryoid body (EB) stage as EBs are 3D aggregates of PSCs that undergo initial developmental specification resembling the pre-gastrulating embryo. This way, a mimicry of the embryonic development is possible with EB formation for the organ in question and their growth *in vitro* allows for an exposure to small molecules to induce particular cellular identities. This results in their differentiation into a 3D self-organized tissue [66]. Self-organization for organoid formation includes underlying mechanisms such as "cell sorting out" and spatially restricted lineage commitment which are highly linked to developmental biology [66].

"Cell sorting out" describes the movement of cells into different domains. This is a key process inherent to tissue patterning that can occur *in vitro* based on *in vivo* events such as morphogenetic cell movements according to distinct adhesive properties of each cell type. Cell adhesion molecules such as E-cadherins, catenins, actin polymerization, and other cell linking proteins are responsible for the establishment of strong cell-cell interactions that regulate cell movements and eventually cell sorting [69]. Naturally, the development of a more complex and robust organoid model is highly dependent on the correct establishment of the ideal cell-cell and cell-ECM interactions. Both aspects will potentiate not only a better resemblance of the organ *in vivo* by activating the necessary signalling pathways that can be dependent on physical properties but also help increase the organoid complexity, where differentiated cells are directed to the correct position while still following major embryogenesis events.

Spatially-restricted cell-fate decisions are also tightly connected with the correct assembly and self-organization of cells in an *in vitro* setting. Stem cell division orientation, the interchange between symmetric and asymmetric divisions along with the rearrangement of differentiated daughter cells to specific locations are all in the basis of spatially-restricted lineage commitment. This process relies on the differentiation of progenitors into more differentiated progeny, which are then confined in the tissue by its organization and orientation, where daughter cells will then be forced into a more superficial position that will promote their subsequent differentiation [66]. This process is very significant as it allows the organoid to achieve a stratified and layered structure, facilitating the display of organo-specific functions. In Figure 1.6 these events can be visualized and further understood.

1.3.1 State of the art

As a first step in the field, James Rheinwald and Howard Green described the long-term culture of human cells for the first time in 1975, by combining freshly isolated keratinocytes with irradiated mouse 3T3 fibroblasts [70]. Furthermore, Mina Bissell and colleagues were the first to make a 3D laminin-rich matrix derived from the mammary gland that resembled an organoid, with observation of morphogenesis *in vitro* [71], [72].

However, the kick-start in the generation of organoids *in vitro* was in 2008 by Yoshiki Sasai's group, who were able to develop 3D cerebral cortex tissue from PSCs [73]. This was contemporaneous with the

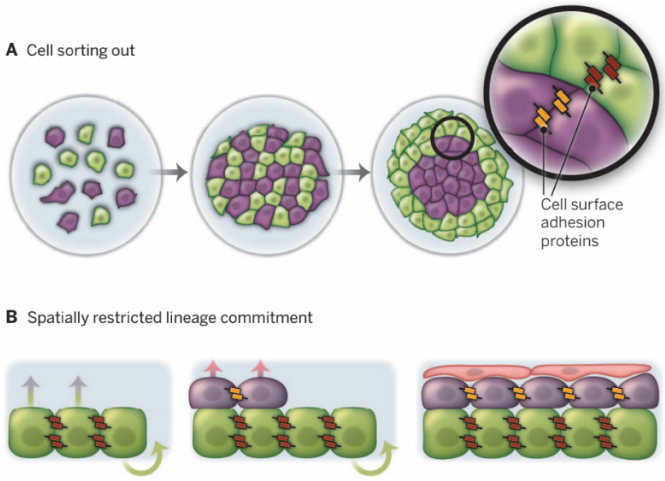

Figure 1.6: Principles of self-organization. Green cells: Progenitors. Purple cells: Differentiated progeny. Pink cells: Further differentiated progeny. Adapted from reference [66].

work of Hans Clevers's group in 2009 that proved that adult intestinal stem cells could form organoids when cultured in 3D, in Matrigel [74]. Later on, a very mediatic case study was reported on the development of "human mini brains" by Lancaster's group in 2013, generated from hiPSCs upon growth in Matrigel, providing a new 3D model for microcephaly [75].

As organoids can be derived from hiPSCs either from healthy donors or patients, using Clustered Regularly Interspaced Short Palindromic Repeats (CRISPR)/CRISPR-associated system (CRISPR-Cas9) technology to correct a single mutation has been accomplished in 2013 for disease modelling. Using intestinal organoids isolated from two different cystic fibrosis patients, restoration of the cystic fibrosis transmembrane conductance regulator (CFTR) gene function in the swelling assay was demonstrated [76]. This also potentiated the first application of an organoid model to personalized medicine, where patient-derived organoids with a very rare CFTR mutation with no known treatment were screened for known cystic fibrosis drugs with a successful outcome, allowing the patient to be safely treated [77]. Taken together, these incredible developments and the work being accomplished daily in the cardiac field indicate how cardiac organoid technology could have a severe impact on better understanding several cardiac disease mechanisms, which could potentiate new personalized medicine approaches.

1.4 Human Cardiac Organoids

Given the definition of an organoid, a human cardiac organoid should comprise several crucial aspects as: **(i)** be composed of multiple heart-specific cell types, **(ii)** be capable of recapitulating heart-specific functions and **(iii)** self-organize structurally and spatially resembling cardiogenesis events. This way, the challenge in obtaining a fully functioning cardiac organoid lies on the high complexity of the human heart. Specifically, the many different cell types present, their different embryonic origin, distinct structural, biochemical, mechanical and electrical properties for the functionality of the heart. Nevertheless, human cardiac organoids (hCOs) have shown a great capacity to establish a cardiac crescent-like structure with temporal and spatial accuracy, allowing for the identification of the FHF and SHF domains *in vitro* [23,78].

In general, cardiomyocytes are grown in 2D culture systems where they adhere and function accordingly. The limitations of turning to a flat surface can be translated in a lack of contractile movement and alignment of the human cellular structure [79]. In this field, two major techniques can be highlighted: scaffold-free and scaffold-based approaches. The first potentiate and rely on cellular self-assembly and organization in the absence of external cues, where cell-cell interactions play a major role. The scaffold-based approaches aim to provide structural support either from synthetic polymers or natural matrixes that mimic the ECM, promoting cell-ECM interactions [80]. In the context of tissue engineering, both approaches have been successfully applied to obtain 3D structures of CMs.

Even though organoids are a much more complex subject, the achievements in 3D cardiac cell culture are relevant as they have been contributing significantly for the optimization and generation of a cardiac organoid platform. In Figure 1.7, the first model is created by cell seeding in a hydrogel mold of either collagen, Matrigel or fibrin, using structural pillars, commonly referred to as an engineered heart tissue (EHT). Cell sheet technology is also depicted, where a 3D structure can be obtained through the stacking of cell layers cultured in a thermorresponsive polymer. A scaffold-free technique is also illustrated, namely the hanging drop technique, which generates cardiac spheroids from gravity formation of small droplets [29]. Naturally, underlying each technique is a set of intrinsic advantages and disadvantages, which need to be taken into consideration regarding the model's purpose and future application. A general overview of positive and negative features attached to each methodology is presented in Table 1.2.

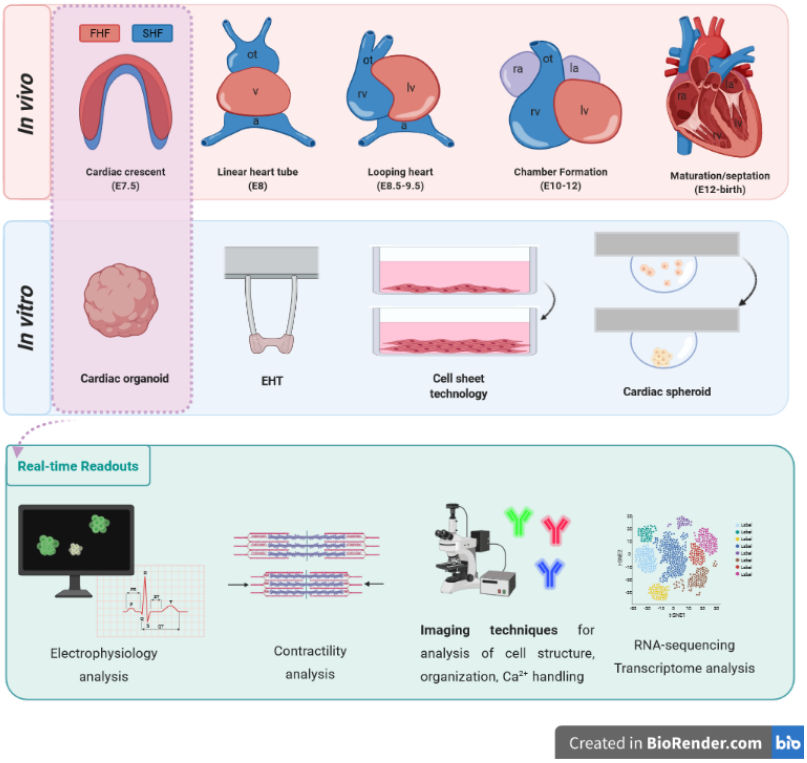

Figure 1.7: Technologies used to culture cardiomyocytes in 3D. Cell seeding in a mold made from hydrogels (EHT). Cell sheet technology for culturing cells in layers. Hanging drop technique to obtain cardiac spheroids. Created with BioRender.com.

Table 1.2: Advantages and disadvantages for each 3D-culture technology used with cardiac cells [1–3].

Method	Cell types used	Advantages	Disadvantages
Scaffold mold (EHT)	- Embryonic chick CMs [81]	Shape can be adapted for specific application (larger models for regenerative medicine and smaller for drug screening)	Higher number of cells per tissue needed
	-Neonatal rat CMs [82] - hESC-derived CMs [83]	Hydrogel can be adapted for organotypic functions (vascularization, stifness)	Limited diffusion properties Risk of breaking
	- hiPSC-derived CMs [52, 84, 85]	Long-term stability	Potential scaffold interference with assays
		Simple multiplexed functional readouts	High degree of experimental artefact
Cell sheet Technology	- Rat neonatal cardiac cells [86] - Mouse cardiac progenitor cell [87]	Mechanical and electrical organotypic functions assays, force assessments	Thickness limitation to three layers [89]
	- Mouse embryonic stem cell (ESC)-derived CMs, neonatal mouse CFs [88]	Avoids using proteases (trypsin, collagenase) which can damage CMs	
	- hiPSC-derived CMs [90, 91] - Human endometrial gland-derived mesenchymal stem cells (MSCs) [92]	Blood perfusion possible for studying the cardiovascular system	Current approaches to generate efficient vascular structures *in vitro* may not be suitable for clinical transplantation [89]
Cardiac Spheroids	- Neonatal rat and mouse CMs [93]	No interference of scaffold proteins with the assays	The absence of ECM factors could impair survival and self-organization of the tissue
	- Human primary adult CMs (co-cultured with EC and iPSC-derived CFs) [94]	Cells are in direct contact with each other from the onset of culture Long-term *in vitro* culture	Significant diffusion gradients of O_2, metabolites and nutrients
	- hiPSC-derived CMs [95] (co-cultured with ECs and hiPSC-derived CFs) [94]	Can be used with smaller number of cells	Small pool number can impair procedures of protein chemistry and ribonucleic acid (RNA) extraction
	- hESC-derived CMs (co-cultured with hESC-derived MSCs) [96]	Can be quickly formed and automatically analysed for drug screening assays	Handling techniques can be difficult as spheroids are free floating and fragile

1.4.1 Previously developed hCO models

3D-engineered hCOs provide a functional model with which to study human cardiac biology and the regenerative phenomena while still maintaining differentiated cell functions for extended periods of time, mimicking the whole organ's dynamics, structure and functional properties [65]. However, due to the absence of a cardiac stem cell niche, designing a successful cardiac organoid model differs from organs like the kidney, or the intestine [74, 97]. Nevertheless, there is evidence stating that, during embryogenesis, fetal mammalian CMs are mononucleated and present a proliferative phenotype which drives the growth of the embryonic heart, which also explains the main role CMs play in the generation of 3D models. [16, 98]. Importantly, the development of hCOs has already potentiated the recapitulation of cardiogenesis *in vitro* [23, 78].

The majority of reports on attempts to mimic the 3D human heart's *in vivo* dynamic have used CMs as the main cell type as opposed to CFs or ECs and a large portion of the existing reports have consisted on simple homotypic CM aggregates [52, 99]. Simpler models of hCOs have focused on specific functions such as general cellular viability, electrophysiological characteristics, Ca^{2+} uptake and responses to external chemical and mechanical cues (in Tables A.1 and A.2, a comprehensive summary of the existing cardiac organoid-like models along with their application and specifications can be found). Of note, in 2020 and 2021, reports on new methodologies have paved way to new and important models with several novel readouts [13, 100–102].

1.4.2 Disease modelling with cardiac organoids

Clearly, low disease relevance and poor *in vivo* recapitulation of human physiology are the major issues current models have and that organoid technology can help overcome. Through the combination of 3D-engineered tissue culture models and genetic engineering techniques, disorders such as DCM [103], Cardiomyopathy-associated Duchenne muscular dystrophy (DMD) [104], hypertrophic cardiomyopathy [105], cardiomyopathy of Barth Syndrome [106] and left ventricular hypertrophy-associated with glycogen accumulation [107] have been successfully studied using heart disease–associated hiPSCs which were previously derived from patients [29].

Regarding inherited arrhythmic disorders, hCOs generated from mutation carrier-derived hiPSC-CMs have successfully modelled contractile pathophysiology with impaired Ca^{2+} cycling and sarcomere insufficiency [108]. Providing a better understanding of relevant functional parameters, hCOs constitute a platform portraying CM-CM interactions via gap junctions, thus enhancing the conduction of both electrical signals and contractile forces. Hence, hCOs have been efficient to model structural arrhythmias allowing for the observation and tracking of rhythmic activation and of arrhythmogenic processes [108]. In cardiac research, isolated organ and tissue preparations have contributed to novel advancements un-

ravelling disease mechanisms; nevertheless, the study of growth, remodelling and disease progression, which could last years, demand that the cells remain viable and functioning for an extended amount of time. Additionally, using organ or tissue preparations does not allow for the recapitulation of the organization of the heart's cell layers and, consequently, the investigation of the fundamental relationships between pressure and volume that characterize the essential function of the heart as a pump [65].

The lack of reports on successfully established physiological and robust hCO platforms for disease modelling is prime evidence of a major limitation in the field. Using hiPSCs as the main source for the derivation of CMs and other subpopulations means that the obtained CMs are very immature, almost equivalent to early gestation cells, as evidenced by the low upstroke velocities of their action potentials, irregular shape, poor sarcomere organization, and gene expression profiles [1]. hiPSC-derived CMs turn to glycolysis for energy production, in the same way as embryonic CMs, in contrast to adult CMs, which tend to use oxidative phosphorylation with fatty acids as the predominant substrate [19]. Evidently, these features can impair the correct modelling of a complex disease not only due to the disparity in phenotype but also in their metabolic activity and function. Some obvious limitations can arise from this if the disease is caused by a mutation in a gene that is only expressed at later stages of development or if the disease only manifests post-natally and has a late onset [36]. Ultimately, given the complex cellular environment and cell type diversity in the human heart, to achieve an optimum and robust disease modelling platform, hCOs should present CM, CF and cardiac EC in a precise cell ratio [29].

Using a 3D cell model enables the preservation of the original shape, polarization, genetic profile, and heterogeneity of the cell population which is possible with hCOs along with the mimicry of the native tissue dynamics and their pathophysiological conditions. 2D and animal models fail to translate regarding PLN mutations as it is suggested that it is difficult to elucidate disease mechanisms exerted by PLN mutations in mice. This is due to the antithetic effects observed in response to complete PLN deletion, which relates to the lower chronotropic reserve of the mouse versus the human heart [109]. This limitation emphasizes the necessity for human-based studies to unravel disease mechanisms associated with PLN R14del.

1.4.3 hCO as a drug screening platform

Cardiac organoids are the ideal technology for the development of improved drug screening platforms, presenting a solution to the non-human model issue as they better mimic human physiology, facilitating regulatory approval [29]. The use of 3D structures could even further facilitate drug screening as the essential readouts (contractile force, Ca^2+ kinetics, reversibility of contractions and cell ultrastructure) can be easily obtained under normal and stressed conditions [1].

Considering that hCOs' lifespan can be increased and therefore cultured for a longer period of time, a more physiological disease model can be obtained and drug screenings are also possible to obtain in

a high-throughput manner. Monolayer culture systems while still being the most cost effective and easy to handle and analyse still do not provide an efficient manner to functionally evaluate CMs electrophysiology in an automated fashion [110]. Consecutively, moving to a 3D system like EHTs has allowed a better mimicry of the *in vivo* microenvironment and a better control of mechanical properties, electrical conductivity, and cell alignment, although still providing a low throughput system [111]. In contrast, hCOs can bridge this gap, providing all the advantages from having a 3D structure with a close resemblance to the human heart while still being cultured individually per well, where several parallel drug screens can be performed, establishing a medium/high-throughput platform.

Readouts such as viability assays through LIVE/DEAD-stained organoid images, adenosine triphosphate (ATP) activity assays, physiological heart beat assays through microscope observation of multi-well plates, ion channel activity measurements through Ca^{2+} transient imaging can be simultaneously obtained and are of extreme relevance in the determination of either electrophysiological and contractility responses to drug exposure [94, 110, 112]. Evidently, another major advantage is the possibility of generating hCOs from patient derived-hiPSCs, which means high throughput readouts can be obtained for a specific disease [110]. Given the late onset of PLN R14del cardiomyopathy in humans, reaching end-stage heart failure cannot be rescued by common guideline recommended drugs. On the other hand, many patients present with more slowly progressive disease, and common heart failure drugs may attenuate progression. As a conclusion, the applications hCOs can potentially have in personalized medicine, drug toxicological screening, disease modelling and regenerative medicine are of great social and economic relevance.

1.5 Thesis Aim and Outline

PLN R14del is associated with severe heart failure and usually presents itself during late adolescence. Mutation carriers present with DCM, which is associated with impaired contractility, arrhythmias, cardiac fibrosis and premature death. To date, the link between impaired contractility, Ca^{2+} mishandling and the profound amount of fibrosis found in the hearts of PLN R14del patients remains unknown along with the link between the mutation and the severity of the cardiomyopathy and arrhythmias generated.

In an attempt to unravel said pathological mechanisms, it is understandable that a 3D model holds greater promise in overcoming many challenges in the field. Organoid structures are expected to present both structural and functional similarities and homologous gene expression profiles compared to their *in vivo* tissue counterpart, representing a high level of organ mimicry achievable in a laboratory setting [67].

Therefore, the following thesis aims to elucidate the molecular mechanisms related to the PLN R14del phenotype in a 3D context establishing cell-based systems for 3D culturing of proliferative CMs derived from hiPSCs. Using this culturing platform, it is expected that the 3D model contributes to a better understanding of the disease phenotype and can constitute a robust middle-high throughput screening platform for novel therapeutic strategies to cure the PLN R14del disease. Accordingly, several goals were proposed for this study, resulting in the following outline:

- develop and setup protocols for the generation of 3D PLN R14del cardiomyopathy models (section 3.1);
- β-adrenergic stimulation of the 3D structures via isoprenaline (ISO) administration using beat rate as a metric (section 3.2);
- immunofluorescence imaging of spheroids and organoids for examination of microtissues' overall morphology, cellular architecture and ratio using CM sarcomeric (α-actinin) and CF (Pro-collagen type 1 (Pro-COL1A1)) markers (section 3.3);
- functional characterization of the cardiac constructs through an analysis of the Ca^{2+} transient properties in whole live 3D cardiac spheroids and organoids (section 3.4).

2

Materials & Methods

Contents

2.1 hiPSC-CMs differentiation

The steps described here for hiPSC and CMs generation until D11 were kindly performed by R.Maas along the duration of the project. Two previously established hiPSC lines (SCVI-273, Sendai virus reprogrammed, peripheral blood mononuclear cells (PBMCs), female [113] and PLN R14del patients [114] were grown to $\sim$90% confluence in a 6 wells cell culture plate. All hiPSCs lines (passage 20-50) were maintained in E8 medium for at least three passages before starting cardiac lineage differentiation with media change occurring every day. hiPSC-CM differentiation was performed using small molecule-based Wnt-modulated protocol previously described starting at D0 with RPMI-B27-ins media supplemented with 8 µM CHIR99021 (CHIR), a canonical Wnt pathway activator (via specific GSK3β) inhibition) [13, 58]. Concentration of CHIR has been tested and varies as each cell line may respond to CHIR treatment differently [57, 58, 100]. On D1, RPMI-B27-ins was added and on D2, an additional 2 mL of the RPMI-B27-ins media was carefully added. On D3, the medium was replaced by 3 mL/well RPMI-B27-ins supplemented with 2 µM Wnt-C59, its exposure lasting 48h. On D5, RPMI-B27-ins media was refreshed. Thereafter, medium was changed every 2 days. At D7, the media RPMI-B27-ins was exchanged for RPMI-B27+ins by adding B27 with insulin (2%) and CMs start to beat on D7-9. The complete formulation and concentration of all media is presented in Table 2.1. Additional information of all media, molecules and material used can be found in supplementary data (Table A.3).

Table 2.1: Media quantitative composition. RPMI - Roswell Park Memorial Institute; DMEM - Dulbecco's modified Eagle's medium; Pen/Strep - Penicillin/streptomycin.

Media / Component	Concentration (vol/vol)
E8 medium	
E8 basal medium	-
Pen/Strep	1%
E8 supplement	2%
RPMI-B27 - ins	
RPMI 1640 + L-Glutamine	-
Pen/Strep	1%
B-27 supplement minus insulin (B27-insulin)	2%
RPMI-B27 + ins	
RPMI 1640 + L-Glutamine	-
Pen/Strep	1%
B27 supplement plus insulin (B27+insulin)	2%
Maturation medium	
DMEM no glucose	-
Pen/Strep	1%
B27+insulin supplement (10X)	2%
KO serum replacement	1%
Maturation Master Mix	10%

2.2 Cardiac spheroids & organoids generation

The protocols elucidated in the following section were developed for this project. Namely, the spheroid generation protocol is a novel methodology resulting from extensive search in literature [28, 78, 101]. Secondly, the organoid production protocol is an adapted protocol from literature [13, 100], with specific modifications and optimizations [101, 102]. Both used control (CTRL) and PLN R14del cell lines.

2.2.1 Spheroid generation

The following protocol (Figure 2.1) was developed to establish a system for 3D culturing of hiPSC-derived CMs with the end goal of obtaining functional human cardiac spheroids. The system can be described

in two main categories: differentiation of hiPSCs into CMs and spheroid formation techniques. The first was defined based on the previously established protocol for massive differentiation of functional hiPSC-derived CMs with up to a 250-fold increase of CM number within 3–5 weeks, developed in our lab [57]. The spheroid handling techniques were designed and studied from previously developed protocols [28, 78, 101].

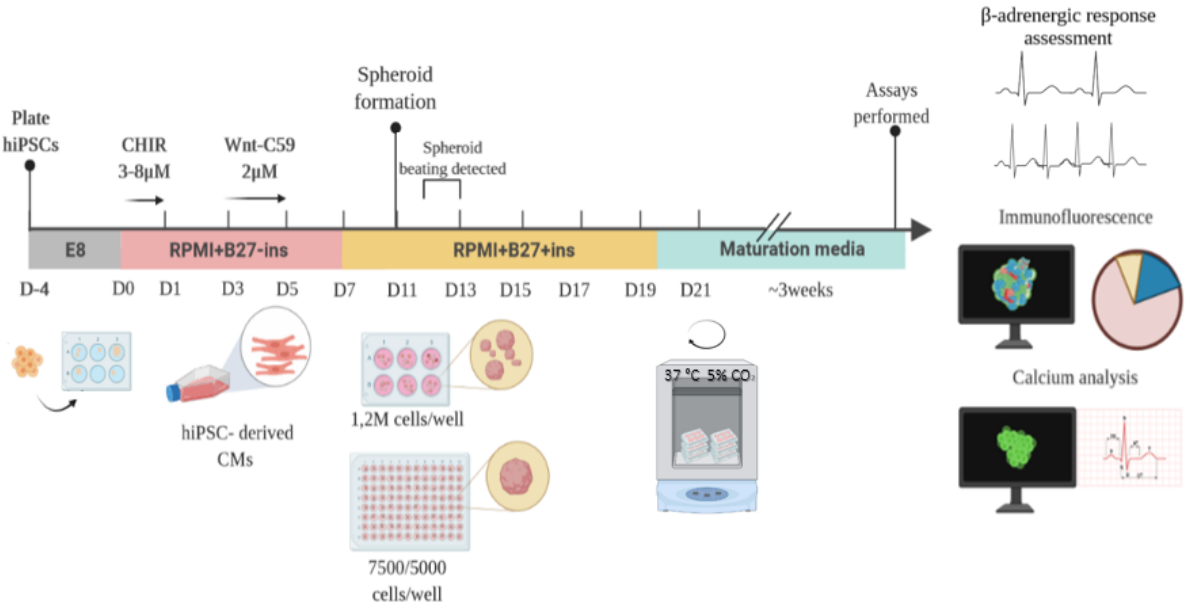

Figure 2.1: Schematic diagram depicting the differentiation protocol used including its timeline along with the main steps of the spheroid generation protocol. Created with Biorender.com.

At D11, wells that contained more than 80% beating cells were treated with TrypLE Select Enzyme 10X at 37° C for 10-15 minutes (0,75 mL/well in a 6-well plate). After incubation, the cells start to loosen and possibly detach and this can be easily checked under the microscope. CMs were flushed from the bottom with 2 mL of RPMI-1640 medium, previously warmed in water bath, and cell suspensions were collected into labelled tubes. Subsequently, the tubes were centrifuged at 300xg for 3 min and the supernatant carefully aspirated. The pellet was resuspended in 1 mL of RPMI-B27+ins supplemented with 10% Knockout (KO) serum replacement, and 10 mM rho-associated coiled-coil protein kinase (ROCK) inhibitor and the cells were counted with 10 µL Trypan blue solution (0,4%) in glass slides. In a 6 wells plate culture format, spheroid generation was optimized to obtain ∼400 μm diameter structures, resulting in 1.2 million cells per mL of RPMI-B27+ins + ROCK (1:1000). In a 96 wells plate culture format, the number of cells to seed were 7500 and 5000 for 250 µL of RPMI-B27+ins + ROCK (1:1000), allowing for the generation of 1 spheroid per well. After counting the cells in each tube, the solution was transferred accordingly to a 6 wells low attachment plate and a 96 wells round-bottom ultra-low attachment plate and kept on the rotation plate (70 rpm, 37° C, 5% CO_2) until fixation on the final time point. On D12, the spheroids were formed using both formats and spontaneous beating was detected from D12-D13,

2 days after spheroid assembly. Medium exchange took place every 2-3 days with previously warmed media in water bath (37° C) till the spheroids were ready to be fixated and assays performed. To refresh the media, the plates were gently rocked to allow spheroids to move to the centre of the well, tilting the plate in a ∼45° angle. For the 6 well format, 2-3 min should be waited after tilting the plate and for spheroids of a smaller diameter, it was advisable to wait for 3-4 min, for spheroid settling at the bottom. Next, media was pipetted out (∼1 mL for 6 well format and 166 µL in 96 well format), with special attention not to aspirate or disrupt spheroids settled at the bottom and warm media was added in the same amount as it was pipetted out.

To ensure the fidelity of the disease model and enhance electrophysiological and mechanical characteristics of hiPSC-derived CMs, a maturation medium was used [115]. In both formats, the media was changed from RPMI-B27+ins to maturation medium around D19-21, depending on the morphology of the spheroids. For a minimum of 3 weeks (∼D42) prior to the characterization and functionality assays were performed, spheroids were kept in this maturation medium, which was also exchanged every 2-3 days [115].

2.2.2 Organoid generation

The next protocol (Figure 2.2) aimed to establish culture hiPSCs in 3D as EBs prior to cardiac differentiation, to obtain self-organizing hCOs. The system can be described in three main categories: EB formation, hiPSC-CMs differentiation and hCOs culturing. This protocol was based, adapted and optimized according to previously established protocols for the formation of 3D cardiac microtissues and self-organizing hCOs [13, 100–102].

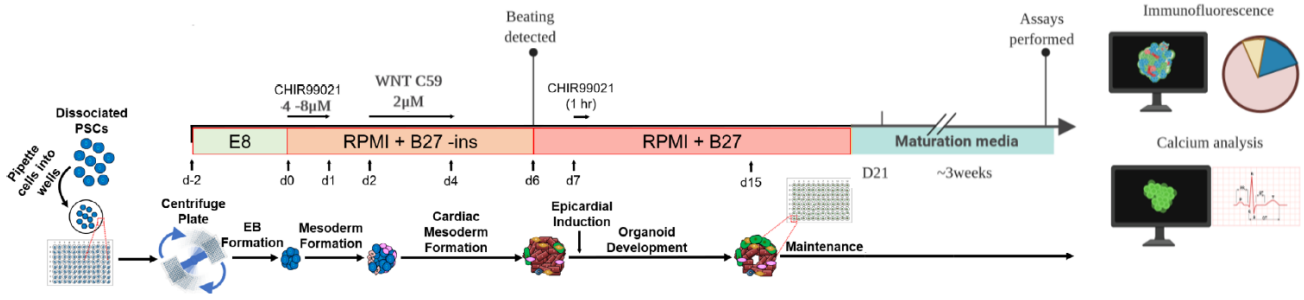

Figure 2.2: Schematic diagram depicting the differentiation protocol used along with the main steps of the human cardiac organoid generation protocol. Adapted from reference [13]. Created with Biorender.com.

EBs formation occurred 2 days prior to the start of cardiac differentiation (D-2). This way, ∼70% confluent hiPSCs were dissociated with 0.5 mM ethylenediaminetetraacetic acid (EDTA) (0,5 mL in 6 well format, 3 mL in a T75 flask) waiting 3-5 min, checking for dissociating cells under the microscope. After EDTA aspiration, each hiPSC cell line was collected with E8 medium supplemented with ROCK inhibitor

(1:1000) in labelled 15 mL tubes. Cell suspensions were centrifuged at 300g for 5 min, supernatant aspirated and cells resuspended in E8 media with RevitaCell (1:100) and counted with Trypan blue solution (0,4%) in glass slides. After counting, hiPSCs were transferred to a round-bottom ultra-low attachment 96 well plate making up 10000, 7500 and 5000 cells per well where the final volume of E8 + ROCK (1:1000) media was 250 µL. The last step for EB formation was centrifugation of the plate after cell seeding at 200xg for 5 min, and the plate was kept in the rotation plate (70 rpm, 37° C, 5% CO_2) throughout the whole experiment, namely until assays could be performed on hCOs. On D-1, E8 medium was refreshed.

The differentiation process was followed as described for the spheroid generation protocol (2.1) with alterations on D2, D6 and D7. Differentiation began on D0, after EB were formed, as 166 µL ($\sim$2/3 of total well volume) of media were removed from each well, adding 166 µL of RPMI-B27-ins supplemented with 4 µM/8 µM of CHIR99021 in each well [100]. On D1, media was exchanged to RPMI-B27-ins. This self-organizing protocol differs from the spheroid one, relying on three sequential Wnt modulation steps of activation/inhibition/activation at specific time points. After activation on D0 occurred using CHIR99021, inhibition ensued on D2 through exposure to Wnt-C59 for 48h. On D4, media was refreshed and on D6 it was exchanged to RPMI-B27+ins. Spontaneous beating was to be detected around D6-D8, 8 days after EB assembly. On D7, after preparation of RPMI-B27+ins media supplemented with 2 µM of CHIR99021, each well was exposed to CHIR99021 for 1h, constituting the last pathway activation step. From D7 onwards, media was exchanged every 2 days until RPMI-B27+ins was exchanged to maturation media on D19-21. hCOs were kept in maturation media for a minimum of 3 weeks ($\sim$D42) until fixation prior to assays execution [115].

A more thorough overview of all reagents and resources used, along with respective additional information is presented in Table A.3. The control and PLN R14del structures obtained from both protocols (hereafter referred to as CTRL/ PLN spheroids and CTRL/ PLN organoids) were treated and subjected to the same assays, at the same time point (D42), namely after being matured for 3 weeks.

2.3 Microtissues experiments

Regarding cardiac spheroids and organoids generated, three assays were performed and analysed:

- β-adrenergic stimulation via ISO administration;
- immunofluorescence imaging of spheroids and organoids using CM sarcomeric (α-actinin, Merck A7811) and CF (Pro-COL1A1, Millipore ABT257) markers;
- Ca^{2+} imaging assay in 3D live structures for cardiac functionality characterization (Cal520 dye, Abcam, ab171868).

2.3.1 Size measurements

Bright-field images were obtained with microscope Olympus CKX41 and further analysed for diameter measurements using the open-source Fiji Software, *ImageJ* (https://imagej.net/software/fiji/).

2.3.2 β-adrenergic stimulation in cardiac spheroids

On the final time point (D42, upon $\sim$3 weeks of maturation), ISO (isoproterenol hydrochloride, Tocris, 1747/100) was diluted in the maturation media at a final concentration of 100 nM and added at 37° C to the wells (6-wells format). CTRL and PLN spheroids were treated in the same conditions and bright-field videos were captured after 15 minutes of exposure to ISO, to be analysed to quantify beats per second.

2.3.3 Immunofluorescence analysis

For immunofluorescence staining, a recently published protocol was used and optimized [116]. The introduction of the nontoxic clearing agent FUnGI in a single incubation step after immunofluorescent staining enhanced fluorescence intensity and preserved fluorescence during storage [116] (see Table 2.2 for clearing agent's composition).

Table 2.2: FUnGI clearing agent composition and supplier information.

Component	Concentration	Source	Identifier
Glycerol	50 % (vol/vol)	Sigma-Aldrich	G9891
dH2O	9.4 % (vol/vol)		
Tris base	10.6 mM (pH 8.0)	Merck	1.08387.0500
EDTA	1.1 mM	Sigma-Aldrich	E4884
Fructose	2.5 M	Sigma-Aldrich	F0127
Urea	2.5 M	MP Biomedicals	02191450-CF

Firstly, spheroids and organoids were collected at the end of maturation stage, by carefully aspirating media and adding cold phosphate-buffered saline (PBS) (1 mL in a 6 well format and 200 µL in 96 well format), with bovine serum albumin (BSA) coated tips into coated tubes. Washed with 10 mL ice-cold PBS, structures were spun down for 3 min at 70xg and 4° C. The spheroids and organoids were re-suspended in 1 mL 4% paraformaldehyde (PFA) solution for 45 min for fixation at 4° C. After fixation and blocking, the microtissues were transferred to a 24 well suspension plate where immunolabeling was performed. The fixation, blocking, immunolabeling, optical clearing and slide preparation sections of the established protocol were followed taking into account the optimizations performed. Throughout the project, several aspects were optimized to achieve the results in section 3.3 and in Table 2.3, this

protocol's troubleshooting is depicted along with the defined optimizations. In Table A.3, supplier information is available for components used in this assay and in Table 2.4, the used antibodies and their concentration are described.

Table 2.3: Troubleshooting for immunofluorescent labeling protocol.

Step	Problem	Solution
Immunolabeling	Poor fluorescence intensity	Increase primary antibodies concentration changing dilution from 1:400 to 1:100 and secondary antibodies dilution from 1:500 to 1:200 (while DAPI/Hoechst dilution remained 1:1000)
FUnGI incubation	FUnGI crystals in the background when imaging	Thaw FUnGI $\sim$3h prior to incubation for optical clearing
	Overflow of microtissues + FUnGI solution upon coverslip placement	Amount of FUnGI solution to be added should be 50-60 to ensure no overflow or bubbles upon coverslip mounting
Slide preparation	Bubble formation upon coverslip placement and pressure applied for coverslip attachment to nail polish	Applying 2 layers of nail polish to the glass slide should be enough amount for either no microtissue damage to occur or no trapped air to remain when coverslip is released

Table 2.4: Antibodies used, dilutions applied upon optimizations and respective additional information.

Antibodies	Dilution	Source	Identifier
Primary antibodies			
Anti-α-actinin, mouse monoclonal	1:100	Merck	A7811
Pro Collagen type 1, rabbit polyclonal	1:100	Millipore	ABT257
Secondary antibodies			
4',6-diamidino-2-phenylindole (DAPI)	1:1000	Thermo	62248
Hoechst 33342	1:1000	Invitrogen	C10245
Alexa Fluor 488 goat anti-mouse	1:200	Invitrogen	A11029
Alexa Fluor 568 goat anti-rabbit	1:200	Invitrogen	A11036

The samples were imaged using Leica SP8 Confocal Microscope at 63x magnification. Confocal images were analysed with the *ImageJ* software where the relative levels of the α-actinin and Pro-COL1A1 proteins were measured.

For cell quantification in the microtissues, DAPI/Hoechst positive cells were counted and used for normalization against the target cell marker of interest (α-actinin and Pro-COL1A1). A MaxEntropy threshold was used to measure the DAPI/Hoechst+, α-actinin+ and Pro-COL1A1+ areas. To sum up, Figure 2.3 represents the main steps of the immunostaining protocol.

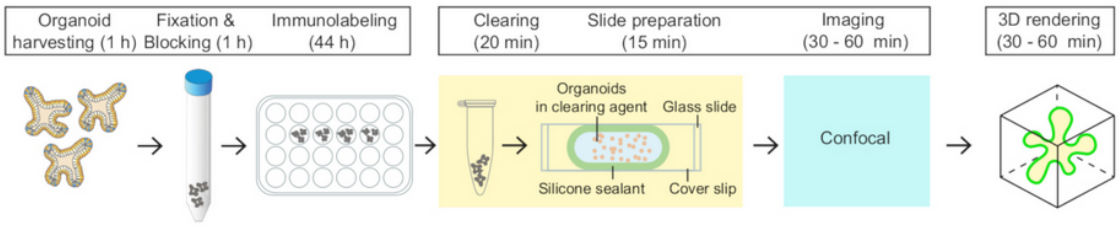

Figure 2.3: Schematic overview of the high-resolution 3D imaging protocol [116].

2.3.4 Calcium assay

To examine electrophysiology in the generated CTRL and PLN constructs, a 3D-calcium handling assay previously developed in our lab was used.

For the calcium assay, the constructs were loaded with the Cal520 dye (1 mg in 362.664 µL DMSO). The Cal520 working solution was prepared on the days of the assay diluting the Cal520 aliquot (2.5 mM stock) 1:1000 with 0,02% Pluronic® F-127 (10% stock, required for successful dye loading according to the manufacturer) in FluoroBrite DMEM media. Importantly, this solution was always protected from light as Cal520 is light-sensitive. Prior to cell loading, this solution should be warmed in the waterbath. Thereafter, the spheroids and organoids were diluted 1:1 with the Cal520 working solution, removing maturation media accordingly (1 mL and 200 µL in 6 well and 96 well format, respectively). The plates already dye-loaded were incubated in 37° C 5% CO_2 for 1h before the calcium assay was performed. During the incubation step, the microscope was warmed to 37° C.

Leica Thunder i8 microscope was used to collect the videos of the Ca^{2+} transient of whole spheroids and organoids with a capture rate of 200 frames per second (8-10 seconds videos) and low exposure. Finally, the video files (AVI) were converted to TIFF format pictures using the *ImageJ* software, and uploaded in the CyteSeer® Automated Video Analysis software (Vala Sciences) (Figure 2.4).

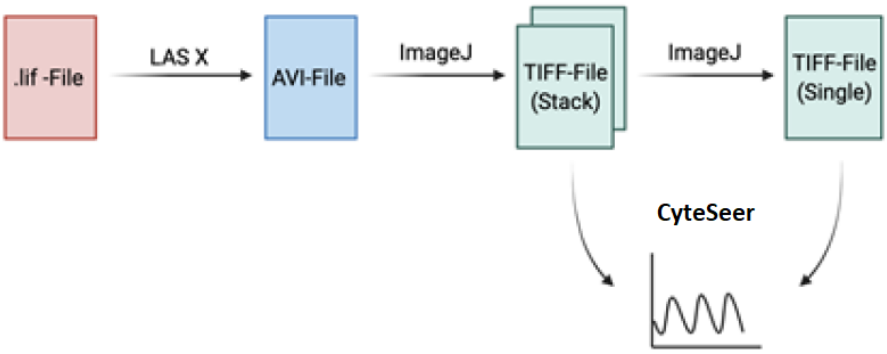

Figure 2.4: Overview of file processing for analysis with CyteSeer®.

2.4 Statistics

Two-group analysis used the Unpaired Student's t test. The p values for significant differences are visualized as: *$p < 0.05$, ** $p < 0.01$, *** $p < 0.001$, **** $p < 0.0001$. Data are expressed and plotted as the Mean $\pm$ SD as indicated in figure legends. The sample size used in each experiment is indicated in the figure legends. Statistical analysis was performed using GraphPad Prism 8.2.0.

3

Results & Discussion

Contents

3.1 Generation of cardiac CTRL and PLN spheroids and organoids

In this project, we aimed to construct a 3D model of the human heart able to recapitulate hallmarks of the PLN R14del cardiomyopathy. To achieve this purpose, two methodologies were developed, optimized and examined.

The spheroid generation protocol is a novel system resulting from extensive literature review that allows for the production of a significant amount of cardiac physiologically-relevant models [28, 78, 101]. The protocol for hiPSC differentiation into CMs for CTRL and PLN cell lines was followed as Figure 3.1 **A** presents with bright-field images taken at the indicated times (Figure 3.1 **C**).

As stated in literature, most successful cardiac expansion is obtained when started between D10 and D14 and spontaneous contraction in hiPSC-derived CMs monolayers is detected on D11 [57]. Consequently, expansion of CMs was started on D11 along with spheroid formation. After cell recovery from replating, CMs began aggregating seeded in 6 wells low attachment and 96 wells ultra-low attachment culture plates. In a 6 wells format, 1.2 million cells proved to generate spheroids of a 400-500 µm diameter (Figure 3.1 **C**). An increase in size upon cardiac expansion was observed and tracked in a 96 wells format as spheroids were cultured individually per well. Spheroid growth was significant from cell recovery and aggregation (D12) to the end of expansion conditions (D19). The detection of size increase in spheroids was expected as demonstrated by the methodology used for cardiac expansion in this project [57, 58]. Using 5000 or 7500 as the cell seeding number in 96 wells format (Figure 3.1 **E**) showed no significant differences in the size obtained at D19 or in functionality in the following assays. Withal, 7500 cells presents no significant diameter change over the course of the experiment for both cell lines, whilst 5000 cells condition showed a statistically significant increase, possibly indicating that cell-cell contact could be inhibiting CM proliferation as stated in previous reports [58]. Thus, 5000 can be considered as a more valuable option to use as cell seeding number given that spheroids from both cell lines were established and showed significant growth overtime with beating activity.

Spontaneous beating was detected after 24-48h of plates incubation in the rotation plate (Figure 3.1 **G**). Functional spheroids were successfully established as a significant amount of spheroids ($\sim$80%) first started beating after aggregation (D12). Before maturation conditions were applied (D19), 99% showed regular beating. This was observed for both cell lines which supports the robustness and reproducibility of the differentiation and spheroid generation techniques used (Figure 3.1 **G**). Furthermore, at the final time point (D42) after maturation, the beat rate was measured for both conditions, validating the functionality of the spheroids generated.

Secondly, a different technique was used to focus on establishing a system for 3D culturing of hiPSCs as EBs prior to cardiac differentiation. The end goal of using this different protocol was to obtain a more organoid-like functional structure in the sense that self-organization throughout differentiation in 3D would be possible. A system was adapted from established methodologies in order to create self-

organizing morphologically complex hCOs from hiPSCs [13, 100, 102], according to the timeline presented in Figure 3.1 **B**. hiPSCs aggregation 2 days prior to the start of the differentiation process allows for cardiac differentiation to occur in 3D. The hiPSCs were assembled into EBs in ultra-low attachment 96-well plates after plate centrifugation and 48h incubation (37° C, 5% CO_2) in the rotation plate. The organoids were first kept in an incubator during organoid generation and maintenance. Nevertheless, it was noted that hCOs were not increasing in size and showed an abnormal development attributed to poor medium quality (Figure 5B from the work of Baillie-Johnson et al. [117]). Hence, an adjustment was made for optimized hCOs generation and, for all subsequent experiments and batches analysed in this study, the plates were kept in a rotation plate instead. This proved to enhance proper EB aggregation, size increase and appropriate cardiac differentiation. Allowing for a proper flow of the small molecules and media used, this adjustment circumvented the significant diffusion gradient possibly underlying these problems and more homogeneous hCOs exposure to the components and nutrients was possible. In Figure 3.1 **D**, whole mount bright-field images of developing hCOs over the course of the experiment show that both CTRL and PLN cell lines were expanding during the experiment, being kept in the rotation plate similar to the cardiac spheroids plates.

Using a 96 wells format, diameter increase was tracked during the differentiation and expansion processes from CHIR induction day (D0) to D8. This day was used for size tracking as literature reports that beating would be first detected on D6. On D7, confocal microscopy should show that sarcomeres would start developing [13]. A significant diameter increase was detected for both cell lines using 5000 and 7500 as cell seeding numbers (Figure 3.1 **F**), endorsing the use of the same numbers for 96-well setup in spheroid formation. Again, the identification of organoids growth was expected as cardiac expansion capacity was enhanced with the medium used for cardiac expansion in this project [57, 58]. Albeit, following Lewis-Israeli et al. [13], 10 000 hiPSCs were seeded in each well. This condition generated abnormal EBs with irregular morphology along development, whose structure was associated with a too high number of cells (Figure 5B from the work of Baillie-Johnson et al. [117]). Furthermore, this condition also reported a much less significant diameter increase overtime (Figure 3.1 **F**). This can be explained by the possible diffusion gradient of small molecules and nutrients associated with 3D structures during the differentiation process and media refreshing being more striking given the higher cell number. This could easily have an influence on impairing development of hCOs.

The previous report used to set up this methodology claimed that on D10, robust and regular beating should be established and on D15 clear sarcomere assembly identified [13]. Therefore, on D8 and D15, hCOs were evaluated according to their beating activity, presenting a behaviour in concordance with literature [13]. Using merely 5000 and 7500 hiPSCs per well allowed for the detection of beating activity on D6-D8 increasing to $\sim$80% on D15 (Figure 3.1 **H**). In a previous report, cardiac lineage formation on D15 was evaluated upon exposure to CHIR (1 µM, 2 µM, 4 µM, 6.6 µM, and 8 µM), revealing that

4 µM condition resulted in the highest CM content [13]. It is stated that the self-organizing method can be associated with endogenous morphogen production, explaining a higher CM content with a lower concentration of CHIR, compared with the one used in cardiac lineage monolayer differentiation [118]. This way, since CHIR concentration is cell-line-dependent [57, 58], CHIR concentrations of the 24h exposure on D0 were tested (4 µM and 8 µM) [13, 100]. Indeed, a significantly higher amount of hCOs were beating on D15 having been exposed to 4 µM of CHIR for 24h on D0 in comparison with the hCOs exposed to 8 µM (Figure 3.1 **H**). Thereafter, taking these results into account, for all subsequent batches analysed, 5000 and 7500 hiPSCs were seeded in the 96 wells plate and 4 µM of CHIR was used for the start of cardiac differentiation, since the response to both concentrations tested was similar in both CTRL and PLN cell lines (Figure 3.1 **H**).

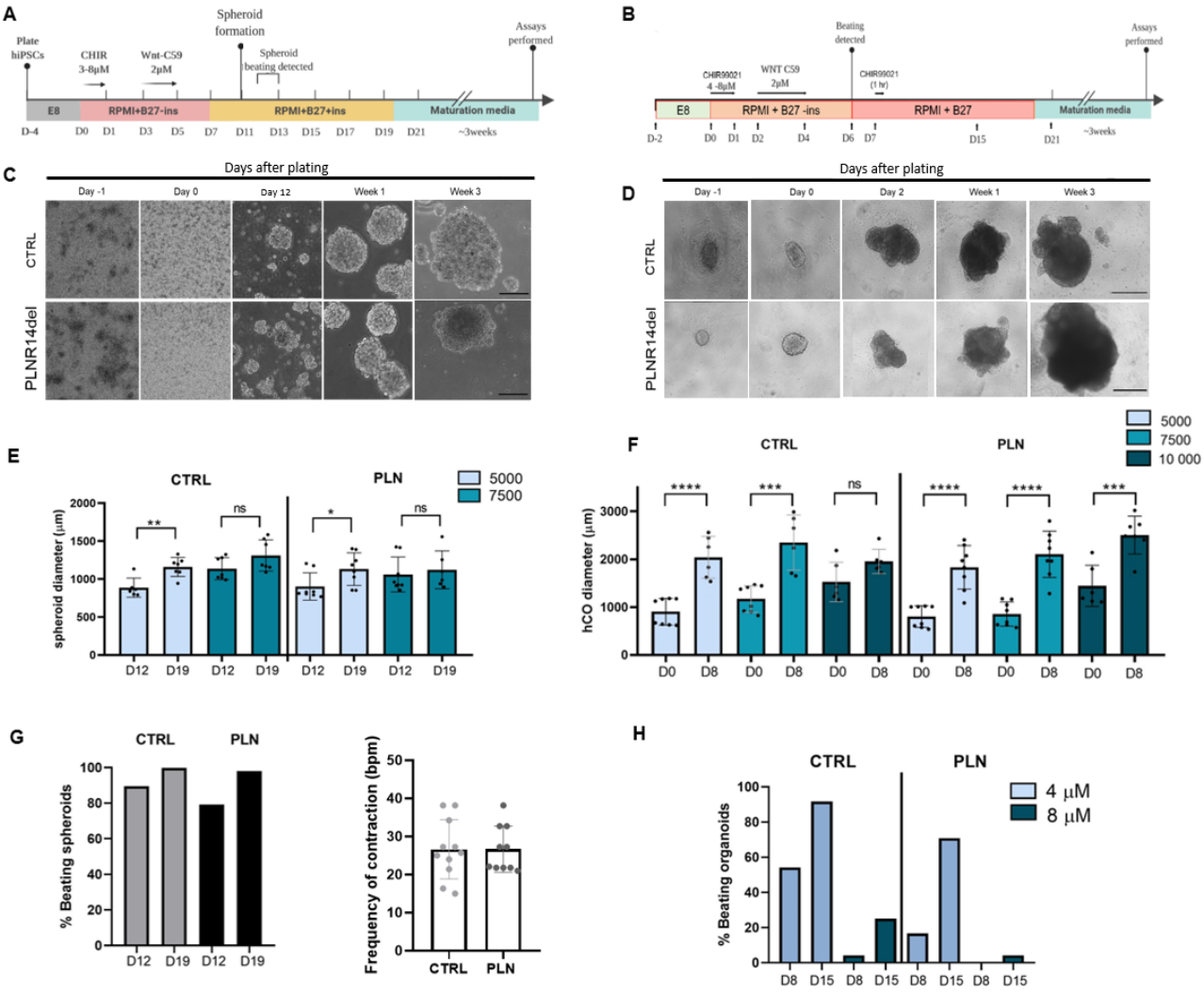

Figure 3.1: Generation of cardiac spheroids and cardiac organoids from CTRL and PLN R14del hiPSCs. **A**: Cardiac differentiation protocol including spheroid generation steps; **B**: Cardiac differentiation while self-assembling hCOs are generated; **C**: Bright-field images of developing CTRL and PLN spheroids over the course of the experiment (6 wells format). Scale bar: 400 µm; **D**: Brightfield images of developing CTRL and PLN hCOs throughout the differentiation process. Scale bar: 1000 µm; **E**: Quantification of spheroid diameter overtime, according to cell number seeded on a 96 wells format (3 independent biological replicates, n = 8 spheroids per condition, value = mean ± s.d., two-tailed, unpaired t-test, ns: no significance, *$p < 0.05$, **$p < 0.001$); **F**: Quantification of organoid diameter overtime, according to cell number seeded (3 independent biological replicates, n = 8 organoids per condition, value = mean ± s.d., two-tailed, unpaired t-test, ns: no significance, ***$p < 0.001$, ****$p < 0.0001$); **G**: Percentage of beating spheroids from D12 to D19 (3 independent biological replicates). Quantification of the contraction frequency of CTRL and PLN spheroids at D42 (3 independent biological replicates); **H**: Percentage of beating hCOs from D8 to D15 in exposure of different concentrations of CHIR on D0 (2 independent biological replicates).

As previously mentioned, the formation of 3D cardiac spheroids occurs upon CMs differentiation and expansion from CTRL and PLN hiPSCs [57]. This method constantly yields a significant amount of functional spheroids for both CTRL and PLN R14del cell lines. This way, it comprises a robust, low-cost

and relatively easy to replicate middle-high throughput platform. A great advantage is the ability to keep spheroids in culture for a considerable period of time, when they are subjected to physiological and functionality assays, which is a feature of great importance when evaluating adult phenotypic pathological features.

Regarding hCO culture, the methodology used in this project allowed for several readouts to be performed on CTRL and PLN hCOs in an automated fashion, being cultured individually per well. The structures obtained were differentiated in 3D, which allowed for cellular self-organization *in vitro* thus, providing a more organoid-like model. Besides showing heart-specific functionality with beating activity detected, it was also cultured for a considerable amount of time, comprising a high-throughput drug screening platform.

3.2 Cardiac spheroids responsive to β-adrenergic stimulation

After setting up the spheroid system, an evaluation of the constructs' response to β-adrenergic stimulation was performed. For this purpose, a cardioactive drug widely used clinically was selected - isoprenaline (isoproterenol hydrochloride) [34, 119]. As isoproterenol is a β-1 and β-2 adrenergic receptor agonist, it binds to the β-adrenergic receptors. When this happens, a G-alpha stimulatory second messenger system is activated, resulting in activation of adenylate cyclase. This enzyme subsequently converts intracellular ATP to cyclic AMP (cAMP) which activates PKA. This way, activated PKA phosphorylates LTCC in CMs and enhances Ca^{2+} release from the SR via RYR2 channels (see Figure 1.3 step 8). Ultimately, this significant increase in intracellular Ca^{2+} concentration translates in heart rate acceleration given the positive inotropic and lusitropic effects of ISO [34, 35].

In Figure 3.2, it can be seen that CTRL and PLN spheroids presented a $\sim$2.1-fold increase of beating frequency upon administration of ISO. A previous report has demonstrated the same behaviour in hiPSC-CMs cardiac organoids [28], while another one using human heart slices showed a $\sim$2.04-fold increase in contractility [120], which is comparable to the measurements obtained in the present assay. Notably, these results are in concordance with human heart measurements upon isoproterenol administration [121].

Overall, the response to ISO administration indicates that the β-adrenergic signaling pathways in hiPSC-CMs within the cardiac spheroids are intact, as a physiologically relevant stimulation is detected. Physiological responses to isoproterenol have also been correlated with tissue maturity when using the same maturation media and time exposure to it as used in this project [115, 122]. Thus, appropriate hiPSC-CMs maturity can be inferred.

Consequently, this proof-of-concept experiment of drug responsiveness in the 3D models generated validates the potential physiological functionality. Therefore, this indicates the applicability of the method

for possible evaluation and comparison of pathological features between the CTRL and PLN spheroids.

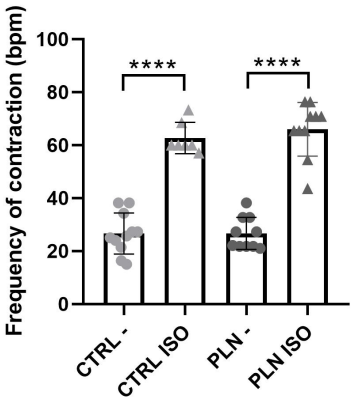

Figure 3.2: Quantification of the contraction frequency of CTRL and PLN spheroids untreated (-) and treated (ISO) with 100 nM of isoprenaline (3 independent biological replicates, n=10 spheroids per condition, value = mean $\pm$ s.d., two-tailed, unpaired t-test, ****p $<$ 0.0001).

3.3 Heart spheroids and organoids produce cardiac-specific cell lineages

After the generation of 3D cardiac microstructures using both methodologies studied, firstly, we examined overall morphology and cellular architecture by whole-mount immunofluorescence (IF) staining for nuclei (DAPI/Hoechst), CM (α-actinin) and CF (Pro-COL1A1) markers.

A – Cellular architecture Immunostaining and confocal microscopy facilitated the evaluation of spatial organization and cellular composition in the spheroids. As previously stated (section 2.3.3), all 3D constructs analysed for cellular architecture and composition had been fixated on D42, after 3 weeks of maturation. In Figure 3.3 **A**, it is noticeable that CMs showing sarcomeric striation were located throughout the entire spheroid, whereas CFs were found interspersed among CMs. Comparing CTRL and PLN spheroids, cellular sorting and architecture in 3D showed no remarkable difference that could be visualized using this assay. The evaluation of the overall spheroid morphology aligned with previous reports also based on the seeding of hiPSC-derived CMs resulting in similar size structures [94, 123].

As for hCOs, in Figure 3.3 **B**, the self-organization of each cell lineage can be observed and cellular architecture understood using the same CM and CF markers previously specified. Spatial cardiac differentiation was successful and could be observed using CTRL and PLN hiPSCs. Notably, CMs appeared throughout the whole hCO, being more directed towards the perimeter. CFs also seemed to be dispersed in the whole structure. These observations are supported by the report from which the

methodology was mostly adapted from [13]. Notably, the PLN R14del mutation also did not seem to be related to any significant cellular organization alteration.

B – Cellular composition Interestingly, we aimed to quantify the contribution of the different cardiac cell populations to the models obtained (Figure 3.3 **C**, **D**). Evidently, the spheroids were generated from hiPSC-derived CMs whereas the organoids resulted from hiPSCs cardiac differentiation in 3D. This means that disparities in cell ratio were expected between spheroids and organoids as the self-organizing method is associated with a possibly less controlled differentiation process in the EB. Once again, the cellular composition obtained in the spheroids is consistent with other models [49, 101] and, more specifically, CF content complied with the one stated in literature [19]. The cellular ratio quantified for CTRL hCOs is similar to a previous report, from which the fabrication methodology was adapted [13]. The clear variation in both methodologies' cellular content is understandable as the spheroid generation protocol allows for the quality control step of seeding only beating hiPSC-derived CMs. Nonetheless, despite the differences observed, in both systems there is a ∼90% and ∼73% increase in Pro-COL1A1-positive area from CTRL to PLN spheroids and organoids, respectively.

C – Pro-collagen type 1 expression in hiPSC-derived CTRL and PLN CMs Taking the previous observations into account, we questioned whether myocardial fibrosis could be recapitulated in the *in vitro* models obtained, given that this is a hallmark of PLN R14del cardiomyopathy. Cardiac fibrosis is characterized by excessive deposition of ECM proteins in the myocardium, disrupting its architecture and ECC [124]. Collagen is the main component of the cardiac ECM and techniques for measuring circulating myocardial fibrosis biomarkers have been explored given their accessibility and non-invasiveness [42, 125]. The carboxy-terminal propeptide of pro-collagen type 1 is synthesized by CFs and released during the biosynthesis process and deposition of collagen 1, being considered a biomarker of collagen synthesis and cardiac fibrosis [126–128]. Moreover, the serum levels of this propeptide have been positively correlated with the degree of myocardial fibrosis in hypertensive heart disease [124].

Consequently, the images obtained by whole-mount IF staining of 3D structures with single-cell resolution were processed to understand the expression of collagen type 1 (COL1A1) gene in the 3D microenvironment. Pro-COL1A1-positive spheroid area was significantly increased in PLN spheroids at this final time point upon CM expansion and maturation (Figure 3.3 **E**). Similarly, Pro-COL1A1-positive organoid area showed a significant increase when also normalized to DAPI/Hoechst-positive area (Figure 3.3 **F**), with an ample expression of this ECM protein detected around and in between CMs. Looking into previously developed PLN R14del models (table 1.1), this data is supported by a formerly studied mouse model which has showed a ∼2-fold increase in cardiac fibrosis upon analysis of left ventricular sections of WT and PLN R14del mice stained with Masson's trichrome [6]. Moreover, a study using

PLN R14del human ventricle heart slices established that the total amount of fibrosis quantified in microscopic slides for this condition was ∼30-40% [44], sharing a close resemblance to the percentage of Pro-COL1A1 obtained in both cardiac models in this project.

It is statistically significant that COL1A1's expression was elevated in PLN spheroids and organoids compared with CTRL. This way, a possible recapitulation of myocardial fibrosis may be considered where several pathological features intrinsic to cardiac fibrosis can be underlying this phenotypic behaviour. On account of cardiac fibrosis being a scarring event in the myocardium with pathological alterations, these can comprise an increased collagen type 1 deposition followed by cardiac fibroblast activation and transdifferentiation into myofibroblasts [96, 129]. ECM components, being exposed to remodeling of composition and structure, can change the mechanical and structural cardiac microenvironment. Cellular architecture is then distorted and this can modulate the proliferation, migration, activation of CFs and phenotypical switch to myofibroblasts [124, 130]. Once fibroblasts are activated, proliferation and migration capacity are increased and this is accompanied by abundant ECM synthesis and deposition, showing increases in fibrillar collagens in the ECM [126, 129]. Accumulation of fibrillar collagen was also observed in myocardium of DCM hearts [126]. Withal, myofibroblasts are phenotypically modulated and characterized by the expression of α-smooth muscle actin (α-SMA) in organized stress fibers and enhanced migratory, proliferative and secretory properties, being essential to fibrosis formation [42,124,131]. As described, several distinct pathological scenarios can be the reason for a significant enhancement of COL1A1 expression. Besides, an alternative cause for this observation could be unpure differentiation of hiPSC-derived CMs prior to spheroid formation and unpure differentiation process of the hiPSC-EBs.

Important to point out is that, generally, hiPSC-derived CMs often present the main limitation of physiological immaturity which diminishes their fidelity as disease models. Notably, the 3 weeks of exposure to maturation media has been determined as being the time point in which gene expression changes indicated maturity changes in CM electrophysiology, Ca^{2+} handling and contractility [115]. Consequently, the fact that all assays in this project were performed upon this same duration of maturation media conditions can better ensure the fidelity of disease model established. Regarding the last assay performed (section 3.3 C –), the cardiac fibrosis model in our study has taken important variables into account in experiment design such as 3D environment and a relevant cell source, although it is not a complete recapitulation of the human situation.

Regarding the characterization of cellular architecture and composition, this approach presents limitations. Furthermore, for a possible and more assertive cardiac fibrosis evaluation, it also presents important knowledge gaps that do not allow for a proper elucidation on the phenomenon observed. All these shortcomings and how to possibly overcome them will be discussed further ahead (section 4.2).

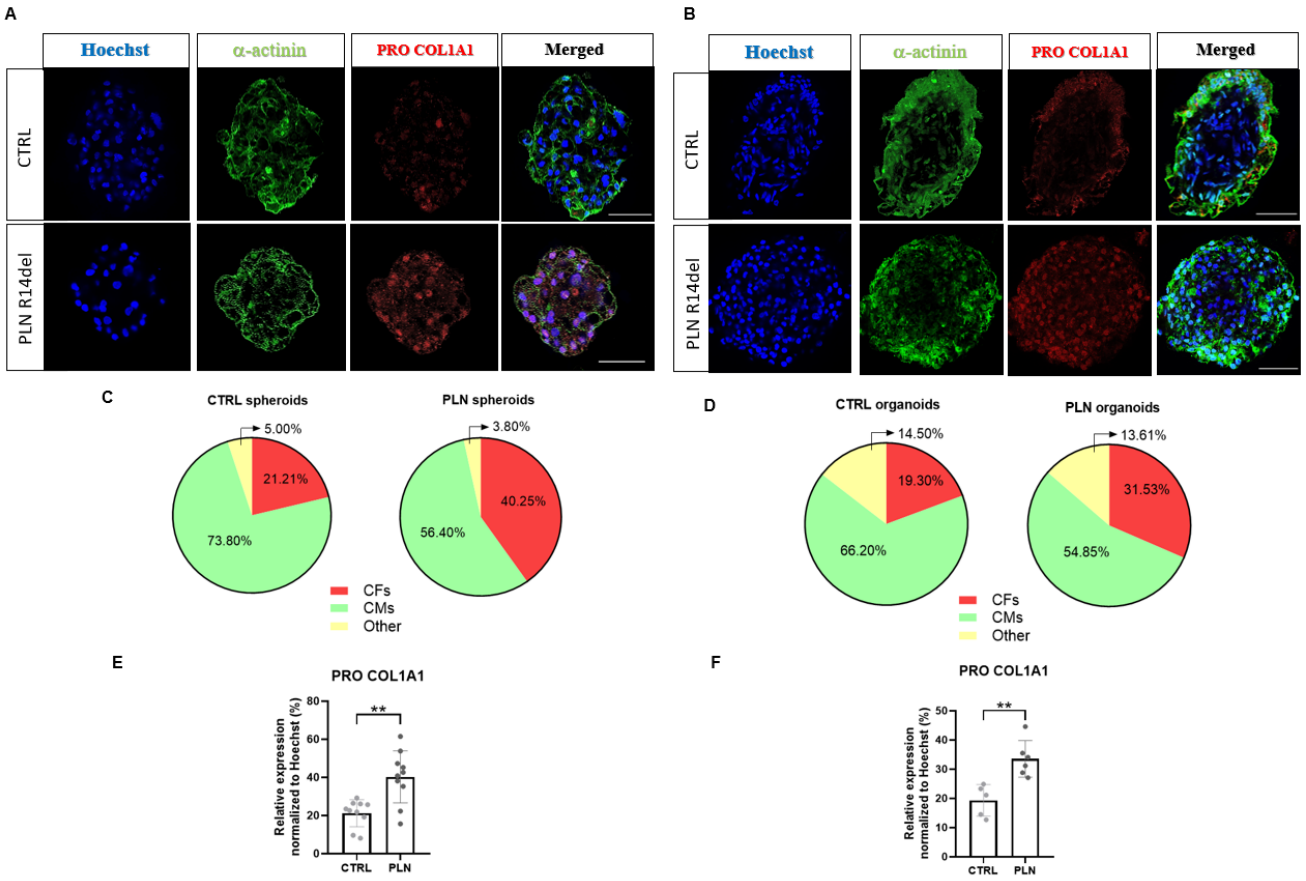

Figure 3.3: Cellular characterization of CTRL and PLN cardiac spheroids and organoids. **A**: Confocal immunofluorescence images of spheroids at D42 for Hoechst (blue), α-actinin (green), Pro-COL1A1 (red) (CTRL in 96-well format and PLN represents the 6-well format). Scale bar: 50 µm; **B**: Confocal immunofluorescence images of hCOs at D42 according to the same staining conditions as **A**. Scale bar: 50 µm; **C**: Pie charts of average cell composition in cardiac spheroids, calculated as the percentage of cells with respective cell marker over all cells by nuclei counting using ImageJ (4 independent biological replicates, n = 10 spheroids per condition); **D**: Pie charts of average cell composition in hCOs, calculated as the percentage of area with respective cell marker over all cells by nuclei counting using ImageJ (2 independent biological replicates, n = 5 CTRL organoids, n= 7 PLN organoids). **E**: Quantification of Pro-COL1A1+ area in the CTRL and PLN spheroids against total cell area (4 independent biological replicates, n = 10 spheroids per condition, value = mean $\pm$ s.d., two-tailed, unpaired t-test, **p=0.001); **F**: Quantification of Pro-COL1A1+ area in the CTRL and PLN hCOs against total cell area (2 independent biological replicates, n = 5 CTRL organoids, n= 7 PLN organoids, value = mean $\pm$ s.d., two-tailed, unpaired t-test, **p=0.0032).

3.4 Calcium handling impairment in PLN R14del models

Besides myocardial fibrosis, malignant ventricular arrhythmias are another key pathological feature of PLN R14del cardiomyopathy in human patients. To further investigate this, Ca^{2+} handling properties were measured, namely, Ca^{2+} handling of CMs in the spheroids and hCOs during ECC, including Ca^{2+} transient pattern and kinetics using fluorescent Ca^{2+} imaging.

Analysis of Ca^{2+} transients in Cal520-loaded 3D spheroids and hCOs allowed the capture of Ca^{2+} sparks overtime for both models obtained in CTRL and PLN conditions (Figure 3.4 **A**, **D**). In Figure 3.4 **B** and **E**, the corresponding Ca^{2+} transients of the constructs can be seen. These results indicate that the spheroids and hCOs generated presented cardiac-like Ca^{2+} transients, which in turn translated into contractions. This observation is supported by the previous data regarding their response to external stimuli, suggesting the hiPSCs' adequate differentiation into cardiac lineage (section 3.2). Together, this data can provide a proper insight and validation of the spheroids and hCOs functionality.

Regarding the Ca^{2+} sparks represented in Figure 3.4 **A** and **D**, it is possible to note that for both PLN models, the Ca^{2+} dye intensity is slightly lower which can be related to the decreased SR Ca^{2+} storage. PLN R14del has a super inhibitory effect on SERCA2a, causing a blockage in Ca^{2+} reuptake in the SR (see section 1.1.2.A). This means that the SR Ca^{2+} content decreases and, consequently, less Ca^{2+} in the SR is available for subsequent contractions. Additionally, in Figure 3.4 **B** and **E**, the CTRL showed regular Ca^{2+} sparks, whereas PLN R14del constructs showed a-synchronized Ca^{2+} sparks, potentially indicating an arrhythmic Ca^{2+} cycling profile [38].

As for Figure 3.4 **C** and **F**, the parameters measured show very similar readouts: Decay Time is significantly increased for PLN as well as CTD25 and CTD75, while Rise Time is not significantly different in PLN spheroids, presenting a lower significant decrease in PLN hCOs than the other parameters. Rise Time is the time it takes for the RYR2 channels to pump Ca^{2+} from the SR back to the cytosol. As such, no considerable difference between PLN and CTRL was expected given that PLN does not interfere with neither these channels nor this process.

Nevertheless, CTD25, CTD75 and Decay Time show a striking decrease for PLN constructs. Decay Time represents the time SERCA2a takes to reuptake Ca^{2+} back in the SR, with CTD25 being the mean of cell-on-cell mask average pixel intensity full-width-75%-maximum time (the difference between the downward part and upward part of the Ca^{2+} peak at 75% maximum time) and CTD75 is the mean of cell-on-cell mask average pixel intensity full-width-25%-maximum time (the difference between the downward part and upward part of the Ca^{2+} peak at 25% maximum time).

CTD25 and CTD75 together account for the overall duration of the Ca^{2+} transient which is shortened in PLN. This is supported by the decreased Decay Time for both models. Several factors could be underlying this response. More specifically, this could also be an indicator on the depressed SR Ca^{2+} content, that will contribute to a lower amount of Ca^{2+} being present in the cytosol for contraction.

Hence, during relaxation, given low Ca^{2+} cytosolic concentration, impaired SERCA2a will pump it into the SR at a higher rate than CTRL, where a greater concentration of Ca^{2+} needs to be reuptaken for relaxation to occur. This has been suggested in literature pointing to DCM hiPSC-derived CMs possibly having a relatively lower Ca^{2+} storage in the SR [132].

Essentially, this assay can indicate there is indeed abnormal Ca^{2+} handling connected with the PLN R14del mutation. The software used for automated image analysis focused on the Ca^{2+} transients within the cytoplasmic area of the cell, which relate primarily to the release and reloading of Ca^{2+} into the SR. This is of important relevance as PLN regulates the SERCA2a pump, precisely responsible for Ca^{2+} reuptake in the SR. Additionally, the high throughput aspect of the software used for analysis is also beneficial as the input could be in a 384-well plate format. However, arrhythmia mechanisms have multi-scale dynamics in the heart and, together, these can lead to life threatening complex arrhythmias. Naturally, the observation of Ca^{2+} transient pattern and kinetics is not enough to properly understand the high frequency of ventricular arrhythmias in PLN R14del cardiomyopathy. Lastly, in section 4.2, there will be suggestions on how to overcome the faults this assay presents.

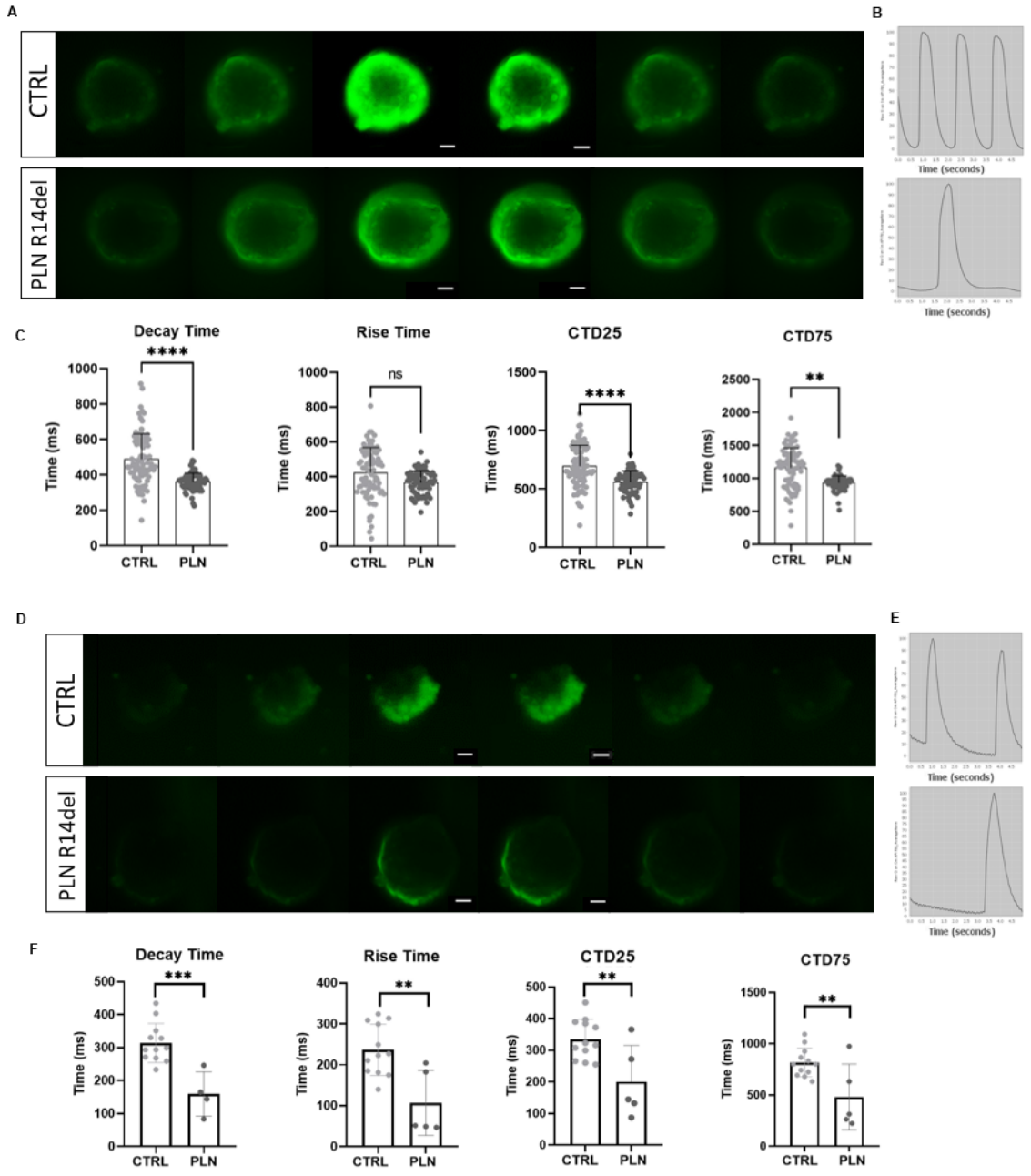

Figure 3.4: Functional characteristics of CTRL and PLN R14del spheroids and organoids. **A**: Ca^{2+} imaging over time in cardiac spheroids, displaying one Ca^{2+} spark for both conditions (96-well format for CTRL and 6-well format for PLN). Scale bar: 20 µm; **B**: The apparent Ca^{2+} intensity of the respective CTRL and PLN spheroids presented in **A**, recorded in 7 sec, with a total of 255 frames; **C**: Quantification of Ca^{2+} transient parameters in CTRL and PLN spheroids: decay time, rise time, CTD25 and CTD75 (6 independent biological replicates, n = 62 CTRL spheroids, n = 40 PLN spheroids, value = mean $\pm$ s.d., two-tailed, unpaired t-test, ns: no significance, **p=0.002, ****p$<$ 0.0001); **D**: Ca^{2+} imaging over time in hCOs, displaying one Ca^{2+} spark for both conditions. Scale bar: 20 µm; **E**: The apparent Ca^{2+} intensity of the respective CTRL and PLN hCOs presented in **D**, recorded in 7 sec, with a total of 255 frames; **F**: Quantification of Ca^{2+} transient parameters in CTRL and PLN organoids: decay time, rise time, CTD25 and CTD75 (2 independent biological replicates, n = 12 CTRL hCOs, n = 5 PLN hCOs, value = mean $\pm$ s.d., two-tailed, unpaired t-test, **p=0.0026 (Rise time), **p=0.0065 (CTD25), **p= 0.0074 (CTD75), ***p=0.0006).

4

Final remarks

Contents

4.1 Study highlights and novelty

Remembering the aims of the project under study (section 1.5), the specific achieved goals were the development of a 3D culturing platform for CMs derived from CTRL and PLN R14del patient; adapting a previous methodology for generating 3D microtissues resembling an organoid-like structure; establishing an immunostaining protocol for intact 3D structures with a set of optimizations successfully applied to an existing report; Ca^{2+} transient parameter analysis was performed when live constructs were loaded with Cal520 and using CyteSeer automated image analysis software.

Thanks to all the troubleshooting performed in the protocols for 3D construct generation, a relatively close resemblance to human physiology and functionality was accomplished (section 3.3 and 3.4). Furthermore, the fact that both systems are from a human origin instead of animal is also greatly beneficial, evading striking non human physiology.

This way, in an attempt to elucidate the still elusive PLN R14del pathophysiology, the assays established were amenable and robust to be performed in a middle-high throughput manner. Even though the experiments allowed for a clear visualization and detection of pathological phenotype features, such as cardiac fibrotic remodelling and Ca^{2+} mishandling, their clear cause, possible direct link or connection to disease severity was not possible to unravel.

4.2 System Limitations and Future Work

Adjustments should be considered to improve on the findings of this study.

On the spheroid generation methodology, it would be valuable to co-culture hiPSC-derived CFs and ECs alongside the CMs. This way, more cardiac cell types would be present and a better representation of the human heart could be obtained. Importantly, for the hCO system, differentiation quality control steps should be added. Namely, Fluorescence-activated cell sorting (FACS) using CM, CF and EC markers would expose the efficacy of cardiac differentiation in time for necessary modifications to be made. In addition, single-cell RNA sequencing at distinct stages of hCO formation could characterize cellular identity.

Regarding the assay for percentage of beating hCOs, more replicates would be necessary. New batches of hCOs would also be useful for the evaluation of ISO exposure in CTRL and PLN models, where it was only tested for the spheroid system. Overall, for all assays performed in this study, more batches of hCOs should be generated and analysed to further validate the conclusions of each experiment.

As for the immunostaining assay, it can be an appropriate method for visualization purposes but not entirely for precise quantification. This can be connected to non homogeneous immunolabelling throughout the whole 3D structure due to difficulties in antibody accessibility to core regions, given that

only intact structures are analysed. For a complete understanding of cellular architecture and composition, staining of more cardiac specific cell types is also crucial (ECs, endocardial and epicardial cells). Additionally, to capture the complete process of cardiac fibrosis, it is essential to incorporate not only CMs but also vascularization as the interactions between various cell types are pivotal for cardiac homeostasis. As discussed before, staining for α-smooth muscle actin (marker for myofibroblasts) could help towards shedding light on the exact fibrosis scenario associated with PLN R14del cardiomyopathy. After considering all the enumerated constraints, the assay performed here also needs further validation for a robust and reliable cellular characterization and evaluation of cardiac fibrosis as it is highly user-dependent. FACS could be an extra assay performed, allowing for a differentiation efficiency quality control step prior to spheroid formation and, on the final time point, for both 3D systems, to better understand cellular content in the models generated. The optimization of a protocol for FACS would be necessary. Crucial steps as spheroid and hCO disruption and antibody selection would need special attention. Structure disruption should allow for a considerable cell number and, consequently, events under evaluation and antibody examination could guarantee appropriate immunolabelling with the least amount of overlapping fluorescence or unstained cells.

Taking into consideration both the complexity of the cardiac arrhythmic scenario in general, and the still unclear cause of the arrhythmic behaviour in PLN R14del cardiomyopathy, more repetitions of the hCOs screening should be done and different assays should be taken into consideration. Possibly, applying the previously established Ca^{2+} quantification assay [133] could help bridging knowledge gaps, measuring Ca^{2+} content of the SR, whether confirming or rejecting the hypothesis presented based on Ca^{2+} content. Another assay that could provide relevant insight into the pathophysiology is single-cell RNA sequencing. This analysis makes it possible to disentangle the complex transcriptional responses across the cellular population in the models [114]. Therefore, gene expression analysis could reveal gene enrichment in disease-relevant pathways that would enlighten the field on this cardiomyopathy mechanism.

4.3 Conclusions

Organoid technology was appointed as Method of the Year in 2017 by Nature given its great potential to advance the understanding of human biology and use for disease modelling, drug screening and personalized medicine [134]. Similarly, the applicability of 3D cardiac models can easily present the same outcomes as organoid technology.

The present study sought to respond to the pressing need for an adult human heart model, having established promising methodologies. The spheroid and organoid systems were successfully developed and adapted, being able to confirmed the pathological features related to PLN R14del cardiomyopathy. Regarding myocardial fibrosis, a fibrotic behaviour was indeed detected in a 3D microenvironment, which is highly relevant in a human disease scenario with various components possibly underlying the readout. Ca^{2+} mishandling was also identified given the irregular Ca^{2+} transient pattern observed in the PLN R14del models, attributed to a wide variety of distinct arrhythmic elements. Unraveling such specific pathological mechanisms should be the focus of research in the future in order to find ways to delay or revert the disease's natural course and severity progression.

Importantly, the poor prognosis associated with PLN R14del cardiomyopathy and the absence of an available therapy is a strong concern. Therefore, both methodologies developed showed potential to be implemented for drug screenings in a patient-specific high-throughput manner using their hiPSCs. Being adjustable to a 96-well format, both platforms enable the culture of one construct per well, where the tracking of individual hCOs under specific conditions is possible. This opens new avenues for target identification and efficient therapeutic intervention, potentiating new personalized medicine approaches.

Bibliography

[1] G. V. Novakovic, T. Eschenhagen, and C. Mummery, "Myocardial tissue engineering: in vitro models," *Cold Spring Harbor perspectives in medicine*, vol. 4, no. 3, p. a014076, 2014.

[2] C. Zuppinger, "3d cardiac cell culture: a critical review of current technologies and applications," *Frontiers in cardiovascular medicine*, vol. 6, p. 87, 2019.

[3] ——, "3d culture for cardiac cells," *Biochimica et Biophysica Acta (BBA)-Molecular Cell Research*, vol. 1863, no. 7, pp. 1873–1881, 2016.

[4] "Cardiovascular diseases (cvds)," https://www.who.int/en/news-room/fact-sheets/detail/cardiovascular-diseases-(cvds), accessed on: 10-04-2021.

[5] G. Gilbert, K. Demydenko, E. Dries, R. D. Puertas, X. Jin, K. Sipido, and H. L. Roderick, "Calcium signaling in cardiomyocyte function," *Cold Spring Harbor perspectives in biology*, vol. 12, no. 3, p. a035428, 2020.

[6] T. R. Eijgenraam, B. J. Boukens, C. J. Boogerd, E. M. Schouten, C. W. van de Kolk, N. M. Stege, W. P. Te Rijdt, E. T. Hoorntje, P. A. van der Zwaag, E. van Rooij *et al.*, "The phospholamban p.(arg14del) pathogenic variant leads to cardiomyopathy with heart failure and is unresponsive to standard heart failure therapy," *Scientific reports*, vol. 10, no. 1, pp. 1–13, 2020.

[7] I. Hof, J. Van der Heijden, E. Kranias, D. Sanoudou, R. De Boer, J. Van Tintelen, P. van der Zwaag, and P. Doevendans, "Prevalence and cardiac phenotype of patients with a phospholamban mutation," *Netherlands Heart Journal*, vol. 27, no. 2, pp. 64–69, 2019.

[8] P. A. Doevendans, P. C. Glijnis, and E. G. Kranias, "Leducq transatlantic network of excellence to cure phospholamban-induced cardiomyopathy (cure-plan)," 2019.

[9] "Pln factsheet," https://en.plnheart.org/pln-factsheet/, accessed on: 29-08-2021.

[10] W. P. Te Rijdt, J. P. van Tintelen, A. Vink, A. C. van der Wal, R. A. de Boer, M. P. van den Berg, and A. J. Suurmeijer, "Phospholamban p. arg14del cardiomyopathy is characterized by phospho-

lamban aggregates, aggresomes, and autophagic degradation," *Histopathology*, vol. 69, no. 4, pp. 542–550, 2016.

[11] P. Horvath, N. Aulner, M. Bickle, A. M. Davies, E. Del Nery, D. Ebner, M. C. Montoya, P. Östling, V. Pietiäinen, L. S. Price *et al.*, "Screening out irrelevant cell-based models of disease," *Nature reviews Drug discovery*, vol. 15, no. 11, p. 751, 2016.

[12] R. J. Mills, B. L. Parker, G. A. Quaife-Ryan, H. K. Voges, E. J. Needham, A. Bornot, M. Ding, H. Andersson, M. Polla, D. A. Elliott *et al.*, "Drug screening in human psc-cardiac organoids identifies pro-proliferative compounds acting via the mevalonate pathway," *Cell stem cell*, vol. 24, no. 6, pp. 895–907, 2019.

[13] Y. R. Lewis-Israeli, A. H. Wasserman, M. A. Gabalski, B. D. Volmert, Y. Ming, K. A. Ball, W. Yang, J. Zou, G. Ni, N. Pajares *et al.*, "Self-assembling human heart organoids for the modeling of cardiac development and congenital heart disease," *Nature Communications*, vol. 12, no. 1, pp. 1–16, 2021.

[14] N. Ferri, P. Siegl, A. Corsini, J. Herrmann, A. Lerman, and R. Benghozi, "Drug attrition during pre-clinical and clinical development: understanding and managing drug-induced cardiotoxicity," *Pharmacology & therapeutics*, vol. 138, no. 3, pp. 470–484, 2013.

[15] Y. Israeli, M. Gabalski, K. Ball, A. Wasserman, J. Zou, G. Ni, C. Zhou, and A. Aguirre, "Generation of heart organoids modeling early human cardiac development under defined conditions," *Available at SSRN 3654622*, 2020.

[16] M. Xin, E. N. Olson, and R. Bassel-Duby, "Mending broken hearts: cardiac development as a basis for adult heart regeneration and repair," *Nature reviews Molecular cell biology*, vol. 14, no. 8, pp. 529–541, 2013.

[17] M. Litviňuková, C. Talavera-López, H. Maatz, D. Reichart, C. L. Worth, E. L. Lindberg, M. Kanda, K. Polanski, M. Heinig, M. Lee *et al.*, "Cells of the adult human heart," *Nature*, vol. 588, no. 7838, pp. 466–472, 2020.

[18] K. E. Hatzistergos, S. Selem, W. Balkan, and J. M. Hare, "Cardiac stem cells: Biology and therapeutic applications," in *Principles of Regenerative Medicine*. Elsevier, 2019, pp. 247–272.

[19] H. D. Devalla and R. Passier, "Cardiac differentiation of pluripotent stem cells and implications for modeling the heart in health and disease," *Science translational medicine*, vol. 10, no. 435, p. eaah5457, 2018.

[20] D. Srivastava, "Making or breaking the heart: from lineage determination to morphogenesis," *Cell*, vol. 126, no. 6, pp. 1037–1048, 2006.

[21] B. G. Bruneau, “Signaling and transcriptional networks in heart development and regeneration,” *Cold Spring Harbor perspectives in biology*, vol. 5, no. 3, p. a008292, 2013.

[22] W. Hasan, “Autonomic cardiac innervation: development and adult plasticity,” *Organogenesis*, vol. 9, no. 3, pp. 176–193, 2013.

[23] G. Rossi, A. Boni, R. Guiet, M. Girgin, R. G. Kelly, and M. P. Lutolf, “Embryonic organoids recapitulate early heart organogenesis,” *bioRxiv*, p. 802181, 2019.

[24] “Three layers of the heart wall,” https://www.thoughtco.com/the-heart-wall-4022792, accessed on: 29-11-2019.

[25] H. Zhang, K. O. Lui, and B. Zhou, “Endocardial cell plasticity in cardiac development, diseases and regeneration,” *Circulation research*, vol. 122, no. 5, pp. 774–789, 2018.

[26] B. Nugraha, M. F. Buono, and M. Y. Emmert, “Modelling human cardiac diseases with 3d organoid,” 2018.

[27] J. Cao and K. D. Poss, “The epicardium as a hub for heart regeneration,” *Nature Reviews Cardiology*, vol. 15, no. 10, pp. 631–647, 2018.

[28] D. J. Richards, R. C. Coyle, Y. Tan, J. Jia, K. Wong, K. Toomer, D. R. Menick, and Y. Mei, “Inspiration from heart development: Biomimetic development of functional human cardiac organoids,” *Biomaterials*, vol. 142, pp. 112–123, 2017.

[29] B. Nugraha, M. F. Buono, L. von Boehmer, S. P. Hoerstrup, and M. Y. Emmert, “Human cardiac organoids for disease modeling,” *Clinical Pharmacology & Therapeutics*, vol. 105, no. 1, pp. 79–85, 2019.

[30] G. M. Wahler, “Cardiac action potentials,” *Cell Physiology Source Book*, pp. 887–898, 2001.

[31] H. Sutanto, A. Lyon, J. Lumens, U. Schotten, D. Dobrev, and J. Heijman, “Cardiomyocyte calcium handling in health and disease: insights from in vitro and in silico studies,” *Progress in biophysics and molecular biology*, vol. 157, pp. 54–75, 2020.

[32] N. Bögeholz, A. Muszynski, and C. Pott, “The physiology of cardiac calcium handling,” *Wiener medizinische Wochenschrift*, vol. 162, no. 13, pp. 278–282, 2012.

[33] J. P. Schmitt, M. Kamisago, M. Asahi, G. H. Li, F. Ahmad, U. Mende, E. G. Kranias, D. H. MacLennan, J. Seidman, and C. E. Seidman, “Dilated cardiomyopathy and heart failure caused by a mutation in phospholamban,” *Science*, vol. 299, no. 5611, pp. 1410–1413, 2003.

[34] M. W. Szymanski and D. P. Singh, “Isoproterenol,” 2018.

[35] S. Alhayek and C. V. Preuss, "Beta 1 receptors," *StatPearls [Internet]*, 2020.

[36] R. P. Davis, C. W. van den Berg, S. Casini, S. R. Braam, and C. L. Mummery, "Pluripotent stem cell models of cardiac disease and their implication for drug discovery and development," *Trends in molecular medicine*, vol. 17, no. 9, pp. 475–484, 2011.

[37] M. M. DeWitt, H. M. MacLeod, B. Soliven, and E. M. McNally, "Phospholamban r14 deletion results in late-onset, mild, hereditary dilated cardiomyopathy," *Journal of the American College of Cardiology*, vol. 48, no. 7, pp. 1396–1398, 2006.

[38] I. Karakikes, F. Stillitano, M. Nonnenmacher, C. Tzimas, D. Sanoudou, V. Termglinchan, C.-W. Kong, S. Rushing, J. Hansen, D. Ceholski *et al.*, "Correction of human phospholamban r14del mutation associated with cardiomyopathy using targeted nucleases and combination therapy," *Nature communications*, vol. 6, no. 1, pp. 1–10, 2015.

[39] K. Haghighi, F. Kolokathis, A. O. Gramolini, J. R. Waggoner, L. Pater, R. A. Lynch, G.-C. Fan, D. Tsiapras, R. R. Parekh, G. W. Dorn *et al.*, "A mutation in the human phospholamban gene, deleting arginine 14, results in lethal, hereditary cardiomyopathy," *Proceedings of the National Academy of Sciences*, vol. 103, no. 5, pp. 1388–1393, 2006.

[40] H.-P. Schultheiss, D. Fairweather, A. L. Caforio, F. Escher, R. E. Hershberger, S. E. Lipshultz, P. P. Liu, A. Matsumori, A. Mazzanti, J. McMurray *et al.*, "Dilated cardiomyopathy," *Nature reviews Disease primers*, vol. 5, no. 1, pp. 1–19, 2019.

[41] A. G. Japp, A. Gulati, S. A. Cook, M. R. Cowie, and S. K. Prasad, "The diagnosis and evaluation of dilated cardiomyopathy," *Journal of the American College of Cardiology*, vol. 67, no. 25, pp. 2996–3010, 2016.

[42] T. R. Eijgenraam, H. H. Silljé, and R. A. de Boer, "Current understanding of fibrosis in genetic cardiomyopathies," *Trends in cardiovascular medicine*, vol. 30, no. 6, pp. 353–361, 2020.

[43] P. M. Seferović, M. Polovina, J. Bauersachs, M. Arad, T. B. Gal, L. H. Lund, S. B. Felix, E. Arbustini, A. L. Caforio, D. Farmakis *et al.*, "Heart failure in cardiomyopathies: a position paper from the heart failure association of the european society of cardiology," *European journal of heart failure*, vol. 21, no. 5, pp. 553–576, 2019.

[44] S. Sepehrkhouy, J. M. Gho, R. van Es, M. Harakalova, N. de Jonge, D. Dooijes, J. J. van der Smagt, M. P. Buijsrogge, R. N. Hauer, R. Goldschmeding *et al.*, "Distinct fibrosis pattern in desmosomal and phospholamban mutation carriers in hereditary cardiomyopathies," *Heart Rhythm*, vol. 14, no. 7, pp. 1024–1032, 2017.

[45] R. R. van de Leur, K. Taha, M. N. Bos, J. F. van der Heijden, D. Gupta, M. J. Cramer, R. J. Hassink, P. van der Harst, P. A. Doevendans, F. W. Asselbergs *et al.*, "Discovering and visualizing disease-specific electrocardiogram features using deep learning: proof-of-concept in phospholamban gene mutation carriers," *Circulation: Arrhythmia and Electrophysiology*, vol. 14, no. 2, p. e009056, 2021.

[46] F. Stillitano, I. C. Turnbull, I. Karakikes, M. Nonnenmacher, P. Backeris, J.-S. Hulot, E. G. Kranias, R. J. Hajjar, and K. D. Costa, "Genomic correction of familial cardiomyopathy in human engineered cardiac tissues," *European heart journal*, vol. 37, no. 43, pp. 3282–3284, 2016.

[47] J. A. Verdonschot, M. R. Hazebroek, P. Wang, S. Sanders-van Wijk, J. J. Merken, Y. A. Adriaansen, A. van den Wijngaard, I. P. Krapels, H.-P. Brunner-La Rocca, H. G. Brunner *et al.*, "Clinical phenotype and genotype associations with improvement in left ventricular function in dilated cardiomyopathy," *Circulation: Heart Failure*, vol. 11, no. 11, p. e005220, 2018.

[48] P. Politi, M. Piccinelli, P. F. Poli, C. Klersy, C. Campana, C. Goggi, M. Viganò, and F. Barale, "Ten years of "extended" life: quality of life among heart transplantation survivors," *Transplantation*, vol. 78, no. 2, pp. 257–263, 2004.

[49] H. K. Voges, R. J. Mills, D. A. Elliott, R. G. Parton, E. R. Porrello, and J. E. Hudson, "Development of a human cardiac organoid injury model reveals innate regenerative potential," *Development*, vol. 144, no. 6, pp. 1118–1127, 2017.

[50] K. Takahashi and S. Yamanaka, "Induction of pluripotent stem cells from mouse embryonic and adult fibroblast cultures by defined factors," *cell*, vol. 126, no. 4, pp. 663–676, 2006.

[51] B. X. Ho, N. M. Q. Pek, and B.-S. Soh, "Disease modeling using 3d organoids derived from human induced pluripotent stem cells," *International journal of molecular sciences*, vol. 19, no. 4, p. 936, 2018.

[52] A. Mathur, P. Loskill, K. Shao, N. Huebsch, S. Hong, S. G. Marcus, N. Marks, M. Mandegar, B. R. Conklin, L. P. Lee *et al.*, "Human ipsc-based cardiac microphysiological system for drug screening applications," *Scientific reports*, vol. 5, p. 8883, 2015.

[53] X. Lian, X. Bao, M. Zilberter, M. Westman, A. Fisahn, C. Hsiao, L. B. Hazeltine, K. K. Dunn, T. J. Kamp, and S. P. Palecek, "Chemically defined, albumin-free human cardiomyocyte generation," *Nature methods*, vol. 12, no. 7, pp. 595–596, 2015.

[54] F. B. Bedada, M. Wheelwright, and J. M. Metzger, "Maturation status of sarcomere structure and function in human ipsc-derived cardiac myocytes," *Biochimica et Biophysica Acta (BBA)-Molecular Cell Research*, vol. 1863, no. 7, pp. 1829–1838, 2016.

[55] P. W. Burridge, E. Matsa, P. Shukla, Z. C. Lin, J. M. Churko, A. D. Ebert, F. Lan, S. Diecke, B. Huber, N. M. Mordwinkin *et al.*, "Chemically defined generation of human cardiomyocytes," *Nature methods*, vol. 11, no. 8, pp. 855–860, 2014.

[56] C. L. Mummery, J. Zhang, E. S. Ng, D. A. Elliott, A. G. Elefanty, and T. J. Kamp, "Differentiation of human embryonic stem cells and induced pluripotent stem cells to cardiomyocytes: a methods overview," *Circulation research*, vol. 111, no. 3, pp. 344–358, 2012.

[57] R. G. Maas, S. Lee, M. Harakalova, C. J. S. Blok, W. R. Goodyer, J. Hjortnaes, P. A. Doevendans, L. W. Van Laake, J. van der Velden, F. W. Asselbergs *et al.*, "Massive expansion and cryopreservation of functional human induced pluripotent stem cell-derived cardiomyocytes," *STAR protocols*, vol. 2, no. 1, p. 100334, 2021.

[58] J. W. Buikema, S. Lee, W. R. Goodyer, R. G. Maas, O. Chirikian, G. Li, Y. Miao, S. L. Paige, D. Lee, H. Wu *et al.*, "Wnt activation and reduced cell-cell contact synergistically induce massive expansion of functional human ipsc-derived cardiomyocytes," *Cell stem cell*, vol. 27, no. 1, pp. 50–63, 2020.

[59] J. W. Buikema, P.-P. M. Zwetsloot, P. A. Doevendans, I. J. Domian, and J. P. Sluijter, "Wnt/β-catenin signaling during cardiac development and repair," *Journal of Cardiovascular Development and Disease*, vol. 1, no. 1, pp. 98–110, 2014.

[60] S. Foulquier, E. P. Daskalopoulos, G. Lluri, K. C. Hermans, A. Deb, and W. M. Blankesteijn, "Wnt signaling in cardiac and vascular disease," *Pharmacological reviews*, vol. 70, no. 1, pp. 68–141, 2018.

[61] X. Lian, C. Hsiao, G. Wilson, K. Zhu, L. B. Hazeltine, S. M. Azarin, K. K. Raval, J. Zhang, T. J. Kamp, and S. P. Palecek, "Robust cardiomyocyte differentiation from human pluripotent stem cells via temporal modulation of canonical wnt signaling," *Proceedings of the National Academy of Sciences*, vol. 109, no. 27, pp. E1848–E1857, 2012.

[62] "Wnt/β-catenin signaling," https://www.cellsignal.com/pathways/wnt-beta-catenin-signaling-pathway, accessed on: 14-04-2021.

[63] X. Lian, J. Zhang, K. Zhu, T. J. Kamp, and S. P. Palecek, "Insulin inhibits cardiac mesoderm, not mesendoderm, formation during cardiac differentiation of human pluripotent stem cells and modulation of canonical wnt signaling can rescue this inhibition," *Stem cells*, vol. 31, no. 3, pp. 447–457, 2013.

[64] C. Freund, D. Ward-van Oostwaard, J. Monshouwer-Kloots, S. van den Brink, M. van Rooijen, X. Xu, R. Zweigerdt, C. Mummery, and R. Passier, "Insulin redirects differentiation from cardio-

genic mesoderm and endoderm to neuroectoderm in differentiating human embryonic stem cells," *Stem cells*, vol. 26, no. 3, pp. 724–733, 2008.

[65] E. J. Lee, D. E. Kim, E. U. Azeloglu, and K. D. Costa, "Engineered cardiac organoid chambers: toward a functional biological model ventricle," *Tissue Engineering Part A*, vol. 14, no. 2, pp. 215–225, 2008.

[66] M. A. Lancaster and J. A. Knoblich, "Organogenesis in a dish: modeling development and disease using organoid technologies," *Science*, vol. 345, no. 6194, p. 1247125, 2014.

[67] Y.-R. Lou and A. W. Leung, "Next generation organoids for biomedical research and applications," *Biotechnology advances*, vol. 36, no. 1, pp. 132–149, 2018.

[68] B. Artegiani and H. Clevers, "Use and application of 3d-organoid technology," *Human molecular genetics*, vol. 27, no. R2, pp. R99–R107, 2018.

[69] M. Simunovic and A. H. Brivanlou, "Embryoids, organoids and gastruloids: new approaches to understanding embryogenesis," *Development*, vol. 144, no. 6, pp. 976–985, 2017.

[70] H. Clevers, "Modeling development and disease with organoids," *Cell*, vol. 165, no. 7, pp. 1586–1597, 2016.

[71] O. W. Petersen, L. Rønnov-Jessen, A. R. Howlett, and M. J. Bissell, "Interaction with basement membrane serves to rapidly distinguish growth and differentiation pattern of normal and malignant human breast epithelial cells." *Proceedings of the National Academy of Sciences*, vol. 89, no. 19, pp. 9064–9068, 1992.

[72] M. Barcellos-Hoff, J. Aggeler, T. Ram, and M. Bissell, "Functional differentiation and alveolar morphogenesis of primary mammary cultures on reconstituted basement membrane," *Development*, vol. 105, no. 2, pp. 223–235, 1989.

[73] M. Eiraku, K. Watanabe, M. Matsuo-Takasaki, M. Kawada, S. Yonemura, M. Matsumura, T. Wataya, A. Nishiyama, K. Muguruma, and Y. Sasai, "Self-organized formation of polarized cortical tissues from escs and its active manipulation by extrinsic signals," *Cell stem cell*, vol. 3, no. 5, pp. 519–532, 2008.

[74] T. Sato, R. G. Vries, H. J. Snippert, M. Van De Wetering, N. Barker, D. E. Stange, J. H. Van Es, A. Abo, P. Kujala, P. J. Peters *et al.*, "Single lgr5 stem cells build crypt–villus structures in vitro without a mesenchymal niche," *Nature*, vol. 459, no. 7244, p. 262, 2009.

[75] M. A. Lancaster, M. Renner, C.-A. Martin, D. Wenzel, L. S. Bicknell, M. E. Hurles, T. Homfray, J. M. Penninger, A. P. Jackson, and J. A. Knoblich, "Cerebral organoids model human brain development and microcephaly," *Nature*, vol. 501, no. 7467, p. 373, 2013.

[76] J. F. Dekkers, C. L. Wiegerinck, H. R. De Jonge, I. Bronsveld, H. M. Janssens, K. M. De Winter-de Groot, A. M. Brandsma, N. W. De Jong, M. J. Bijvelds, B. J. Scholte *et al.*, "A functional cftr assay using primary cystic fibrosis intestinal organoids," *Nature medicine*, vol. 19, no. 7, pp. 939–945, 2013.

[77] A. Saini, "Cystic fibrosis patients benefit from mini guts," *Cell Stem Cell*, vol. 19, no. 4, pp. 425–427, 2016.

[78] P. Andersen, E. Tampakakis, D. V. Jimenez, S. Kannan, M. Miyamoto, H. K. Shin, A. Saberi, S. Murphy, E. Sulistio, S. P. Chelko *et al.*, "Precardiac organoids form two heart fields via bmp/wnt signaling," *Nature communications*, vol. 9, no. 1, pp. 1–13, 2018.

[79] X. Yin, B. E. Mead, H. Safaee, R. Langer, J. M. Karp, and O. Levy, "Engineering stem cell organoids," *Cell stem cell*, vol. 18, no. 1, pp. 25–38, 2016.

[80] B. R. Desroches, P. Zhang, B.-R. Choi, M. E. King, A. E. Maldonado, W. Li, A. Rago, G. Liu, N. Nath, K. M. Hartmann *et al.*, "Functional scaffold-free 3-d cardiac microtissues: a novel model for the investigation of heart cells," *American Journal of Physiology-Heart and Circulatory Physiology*, vol. 302, no. 10, pp. H2031–H2042, 2012.

[81] T. Eschenhagen, C. Fink, U. Remmers, H. Scholz, J. Wattchow, J. Weil, W. Zimmermann, H. H. Dohmen, H. Schäfer, N. Bishopric *et al.*, "Three-dimensional reconstitution of embryonic cardiomyocytes in a collagen matrix: a new heart muscle model system," *The FASEB journal*, vol. 11, no. 8, pp. 683–694, 1997.

[82] W.-H. Zimmermann, M. Didié, G. H. Wasmeier, U. Nixdorff, A. Hess, I. Melnychenko, O. Boy, W. L. Neuhuber, M. Weyand, and T. Eschenhagen, "Cardiac grafting of engineered heart tissue in syngenic rats," *Circulation*, vol. 106, no. 12_suppl_1, pp. I–151, 2002.

[83] D. Zhang, I. Y. Shadrin, J. Lam, H.-Q. Xian, H. R. Snodgrass, and N. Bursac, "Tissue-engineered cardiac patch for advanced functional maturation of human esc-derived cardiomyocytes," *Biomaterials*, vol. 34, no. 23, pp. 5813–5820, 2013.

[84] N. L. Tulloch, V. Muskheli, M. V. Razumova, F. S. Korte, M. Regnier, K. D. Hauch, L. Pabon, H. Reinecke, and C. E. Murry, "Growth of engineered human myocardium with mechanical loading and vascular coculture," *Circulation research*, vol. 109, no. 1, pp. 47–59, 2011.

[85] S. S. Nunes, J. W. Miklas, J. Liu, R. Aschar-Sobbi, Y. Xiao, B. Zhang, J. Jiang, S. Massé, M. Gagliardi, A. Hsieh *et al.*, "Biowire: a platform for maturation of human pluripotent stem cell–derived cardiomyocytes," *Nature methods*, vol. 10, no. 8, pp. 781–787, 2013.

[86] T. Shimizu, M. Yamato, Y. Isoi, T. Akutsu, T. Setomaru, K. Abe, A. Kikuchi, M. Umezu, and T. Okano, "Fabrication of pulsatile cardiac tissue grafts using a novel 3-dimensional cell sheet manipulation technique and temperature-responsive cell culture surfaces," *Circulation research*, vol. 90, no. 3, pp. e40–e48, 2002.

[87] K. Matsuura, A. Honda, T. Nagai, N. Fukushima, K. Iwanaga, M. Tokunaga, T. Shimizu, T. Okano, H. Kasanuki, N. Hagiwara *et al.*, "Transplantation of cardiac progenitor cells ameliorates cardiac dysfunction after myocardial infarction in mice," *The Journal of clinical investigation*, vol. 119, no. 8, pp. 2204–2217, 2009.

[88] K. Matsuura, S. Masuda, Y. Haraguchi, N. Yasuda, T. Shimizu, N. Hagiwara, P. W. Zandstra, and T. Okano, "Creation of mouse embryonic stem cell-derived cardiac cell sheets," *Biomaterials*, vol. 32, no. 30, pp. 7355–7362, 2011.

[89] S. Masuda and T. Shimizu, "Three-dimensional cardiac tissue fabrication based on cell sheet technology," *Advanced drug delivery reviews*, vol. 96, pp. 103–109, 2016.

[90] K. Matsuura, M. Wada, T. Shimizu, Y. Haraguchi, F. Sato, K. Sugiyama, K. Konishi, Y. Shiba, H. Ichikawa, A. Tachibana *et al.*, "Creation of human cardiac cell sheets using pluripotent stem cells," *Biochemical and biophysical research communications*, vol. 425, no. 2, pp. 321–327, 2012.

[91] Y. Haraguchi, K. Matsuura, T. Shimizu, M. Yamato, and T. Okano, "Simple suspension culture system of human ips cells maintaining their pluripotency for cardiac cell sheet engineering," *Journal of tissue engineering and regenerative medicine*, vol. 9, no. 12, pp. 1363–1375, 2015.

[92] N. Hida, N. Nishiyama, S. Miyoshi, S. Kira, K. Segawa, T. Uyama, T. Mori, K. Miyado, Y. Ikegami, C. Cui *et al.*, "Novel cardiac precursor-like cells from human menstrual blood-derived mesenchymal cells," *Stem cells*, vol. 26, no. 7, pp. 1695–1704, 2008.

[93] J. M. Kelm, E. Ehler, L. K. Nielsen, S. Schlatter, J.-C. Perriard, and M. Fussenegger, "Design of artificial myocardial microtissues," *Tissue engineering*, vol. 10, no. 1-2, pp. 201–214, 2004.

[94] L. Polonchuk, M. Chabria, L. Badi, J.-C. Hoflack, G. Figtree, M. J. Davies, and C. Gentile, "Cardiac spheroids as promising in vitro models to study the human heart microenvironment," *Scientific reports*, vol. 7, no. 1, pp. 1–12, 2017.

[95] P. Beauchamp, W. Moritz, J. M. Kelm, N. D. Ullrich, I. Agarkova, B. D. Anson, T. M. Suter, and C. Zuppinger, "Development and characterization of a scaffold-free 3d spheroid model of induced pluripotent stem cell-derived human cardiomyocytes," *Tissue Engineering Part C: Methods*, vol. 21, no. 8, pp. 852–861, 2015.

[96] M.-O. Lee, K. B. Jung, S.-J. Jo, S.-A. Hyun, K.-S. Moon, J.-W. Seo, S.-H. Kim, and M.-Y. Son, "Modelling cardiac fibrosis using three-dimensional cardiac microtissues derived from human embryonic stem cells," *Journal of biological engineering*, vol. 13, no. 1, pp. 1–17, 2019.

[97] S. Reule and S. Gupta, "Kidney regeneration and resident stem cells," *Organogenesis*, vol. 7, no. 2, pp. 135–139, 2011.

[98] K. Kikuchi and K. D. Poss, "Cardiac regenerative capacity and mechanisms," *Annual review of cell and developmental biology*, vol. 28, pp. 719–741, 2012.

[99] O. O. Akintewe, E. G. Roberts, N.-G. Rim, M. A. Ferguson, and J. Y. Wong, "Design approaches to myocardial and vascular tissue engineering," *Annual review of biomedical engineering*, vol. 19, pp. 389–414, 2017.

[100] P. Hofbauer, S. M. Jahnel, N. Papai, M. Giesshammer, A. Deyett, C. Schmidt, M. Penc, K. Tavernini, N. Grdseloff, C. Meledeth *et al.*, "Cardioids reveal self-organizing principles of human cardiogenesis," *Cell*, 2021.

[101] E. Giacomelli, V. Meraviglia, G. Campostrini, A. Cochrane, X. Cao, R. W. Van Helden, A. K. Garcia, M. Mircea, S. Kostidis, R. P. Davis *et al.*, "Human-ipsc-derived cardiac stromal cells enhance maturation in 3d cardiac microtissues and reveal non-cardiomyocyte contributions to heart disease," *Cell stem cell*, vol. 26, no. 6, pp. 862–879, 2020.

[102] L. Drakhlis, S. Biswanath, C.-M. Farr, V. Lupanow, J. Teske, K. Ritzenhoff, A. Franke, F. Manstein, E. Bolesani, H. Kempf *et al.*, "Human heart-forming organoids recapitulate early heart and foregut development," *Nature Biotechnology*, pp. 1–10, 2021.

[103] J. T. Hinson, A. Chopra, N. Nafissi, W. J. Polacheck, C. C. Benson, S. Swist, J. Gorham, L. Yang, S. Schafer, C. C. Sheng *et al.*, "Titin mutations in ips cells define sarcomere insufficiency as a cause of dilated cardiomyopathy," *Science*, vol. 349, no. 6251, pp. 982–986, 2015.

[104] C. Long, H. Li, M. Tiburcy, C. Rodriguez-Caycedo, V. Kyrychenko, H. Zhou, Y. Zhang, Y.-L. Min, J. M. Shelton, P. P. Mammen *et al.*, "Correction of diverse muscular dystrophy mutations in human engineered heart muscle by single-site genome editing," *Science Advances*, vol. 4, no. 1, p. eaap9004, 2018.

[105] T. J. Cashman, R. Josowitz, B. V. Johnson, B. D. Gelb, and K. D. Costa, "Human engineered cardiac tissues created using induced pluripotent stem cells reveal functional characteristics of braf-mediated hypertrophic cardiomyopathy," *PloS one*, vol. 11, no. 1, p. e0146697, 2016.

[106] G. Wang, M. L. McCain, L. Yang, A. He, F. S. Pasqualini, A. Agarwal, H. Yuan, D. Jiang, D. Zhang, L. Zangi *et al.*, "Modeling the mitochondrial cardiomyopathy of barth syndrome with induced

pluripotent stem cell and heart-on-chip technologies," *Nature medicine*, vol. 20, no. 6, pp. 616–623, 2014.

[107] J. T. Hinson, A. Chopra, A. Lowe, C. C. Sheng, R. M. Gupta, R. Kuppusamy, J. O'Sullivan, G. Rowe, H. Wakimoto, J. Gorham *et al.*, "Integrative analysis of prkag2 cardiomyopathy ips and microtissue models identifies ampk as a regulator of metabolism, survival, and fibrosis," *Cell reports*, vol. 17, no. 12, pp. 3292–3304, 2016.

[108] J.-S. Hulot, "Modeling cardiac arrhythmias with organoids," 2019.

[109] F. Cuello, A. E. Knaust, U. Saleem, M. Loos, J. Raabe, D. Mosqueira, S. Laufer, M. Schweizer, P. van der Kraak, F. Flenner *et al.*, "Impairment of the er/mitochondria compartment in human cardiomyocytes with pln p. arg14del mutation," *EMBO molecular medicine*, p. e13074, 2021.

[110] G. Conant, B. F. L. Lai, R. X. Z. Lu, A. Korolj, E. Y. Wang, and M. Radisic, "High-content assessment of cardiac function using heart-on-a-chip devices as drug screening model," *Stem Cell Reviews and Reports*, vol. 13, no. 3, pp. 335–346, 2017.

[111] K. Yue, G. Trujillo-de Santiago, M. M. Alvarez, A. Tamayol, N. Annabi, and A. Khademhosseini, "Synthesis, properties, and biomedical applications of gelatin methacryloyl (gelma) hydrogels," *Biomaterials*, vol. 73, pp. 254–271, 2015.

[112] S. D. Forsythe, M. Devarasetty, T. Shupe, C. Bishop, A. Atala, S. Soker, and A. Skardal, "Environmental toxin screening using human-derived 3d bioengineered liver and cardiac organoids," *Frontiers in public health*, vol. 6, p. 103, 2018.

[113] E. Matsa, P. W. Burridge, K.-H. Yu, J. H. Ahrens, V. Termglinchan, H. Wu, C. Liu, P. Shukla, N. Sayed, J. M. Churko *et al.*, "Transcriptome profiling of patient-specific human ipsc-cardiomyocytes predicts individual drug safety and efficacy responses in vitro," *Cell stem cell*, vol. 19, no. 3, pp. 311–325, 2016.

[114] D. A. Feyen, I. Perea-Gil, R. G. Maas, M. Harakalova, A. A. Gavidia, J. Arthur Ataam, T.-H. Wu, A. Vink, J. Pei, N. Vadgama *et al.*, "The unfolded protein response as a compensatory mechanism and potential therapeutic target in pln r14del cardiomyopathy," *Circulation*, 2021.

[115] D. A. Feyen, W. L. McKeithan, A. A. Bruyneel, S. Spiering, L. Hörmann, B. Ulmer, H. Zhang, F. Briganti, M. Schweizer, B. Hegyi *et al.*, "Metabolic maturation media improve physiological function of human ipsc-derived cardiomyocytes," *Cell reports*, vol. 32, no. 3, p. 107925, 2020.

[116] R. L. van Ineveld, H. C. Ariese, E. J. Wehrens, J. F. Dekkers, and A. C. Rios, "Single-cell resolution three-dimensional imaging of intact organoids," *JoVE (Journal of Visualized Experiments)*, no. 160, p. e60709, 2020.

[117] P. Baillie-Johnson, S. C. Van den Brink, T. Balayo, D. A. Turner, and A. M. Arias, "Generation of aggregates of mouse embryonic stem cells that show symmetry breaking, polarization and emergent collective behaviour in vitro," *Journal of visualized experiments: JoVE*, no. 105, 2015.

[118] A. Sharma, Y. Zhang, J. W. Buikema, V. Serpooshan, O. Chirikian, N. Kosaric, J. M. Churko, E. Dzilic, A. Shieh, P. W. Burridge *et al.*, "Stage-specific effects of bioactive lipids on human ipsc cardiac differentiation and cardiomyocyte proliferation," *Scientific reports*, vol. 8, no. 1, pp. 1–10, 2018.

[119] T. C. Stummann, M. Wronski, T. Sobanski, B. Kumpfmueller, L. Hareng, S. Bremer, and M. P. Whelan, "Digital movie analysis for quantification of beating frequencies, chronotropic effects, and beating areas in cardiomyocyte cultures," *Assay and drug development technologies*, vol. 6, no. 3, pp. 375–385, 2008.

[120] M. Brandenburger, J. Wenzel, R. Bogdan, D. Richardt, F. Nguemo, M. Reppel, J. Hescheler, H. Terlau, and A. Dendorfer, "Organotypic slice culture from human adult ventricular myocardium," *Cardiovascular research*, vol. 93, no. 1, pp. 50–59, 2012.

[121] J. R. Stratton, M. D. Cerqueira, R. S. Schwartz, W. C. Levy, R. Veith, S. E. Kahn, and I. B. Abrass, "Differences in cardiovascular responses to isoproterenol in relation to age and exercise training in healthy men." *Circulation*, vol. 86, no. 2, pp. 504–512, 1992.

[122] K. Ronaldson-Bouchard, S. P. Ma, K. Yeager, T. Chen, L. Song, D. Sirabella, K. Morikawa, D. Teles, M. Yazawa, and G. Vunjak-Novakovic, "Advanced maturation of human cardiac tissue grown from pluripotent stem cells," *Nature*, vol. 556, no. 7700, pp. 239–243, 2018.

[123] P. Beauchamp, C. B. Jackson, L. C. Ozhathil, I. Agarkova, C. L. Galindo, D. B. Sawyer, T. M. Suter, and C. Zuppinger, "3d co-culture of hipsc-derived cardiomyocytes with cardiac fibroblasts improves tissue-like features of cardiac spheroids," *Frontiers in molecular biosciences*, vol. 7, p. 14, 2020.

[124] L. Li, Q. Zhao, and W. Kong, "Extracellular matrix remodeling and cardiac fibrosis," *Matrix biology*, vol. 68, pp. 490–506, 2018.

[125] C. Yang, S. Qiao, Y. Song, Y. Liu, Y. Tang, L. Deng, J. Yuan, F. Hu, and W. Yang, "Procollagen type i carboxy-terminal propeptide (picp) and mmp-2 are potential biomarkers of myocardial fibrosis in patients with hypertrophic cardiomyopathy," *Cardiovascular Pathology*, vol. 43, p. 107150, 2019.

[126] L. S. Neff and A. D. Bradshaw, "Cross your heart? collagen cross-links in cardiac health and disease," *Cellular Signalling*, vol. 79, p. 109889, 2021.

[127] A. G. Raafs, J. A. Verdonschot, M. T. Henkens, B. P. Adriaans, P. Wang, K. Derks, M. A. A. Hamid, C. Knackstedt, V. P. van Empel, J. Díez *et al.*, "The combination of carboxy-terminal propeptide

of procollagen type i blood levels and late gadolinium enhancement at cardiac magnetic resonance provides additional prognostic information in idiopathic dilated cardiomyopathy–a multilevel assessment of myocardial fibrosis in dilated cardiomyopathy," *European Journal of Heart Failure*, vol. 23, no. 6, p. 933, 2021.

[128] B. López, A. González, N. Varo, C. Laviades, R. Querejeta, and J. Díez, "Biochemical assessment of myocardial fibrosis in hypertensive heart disease," *Hypertension*, vol. 38, no. 5, pp. 1222–1226, 2001.

[129] S. Hinderer and K. Schenke-Layland, "Cardiac fibrosis–a short review of causes and therapeutic strategies," *Advanced drug delivery reviews*, vol. 146, pp. 77–82, 2019.

[130] G. A. Figtree, K. J. Bubb, O. Tang, E. Kizana, and C. Gentile, "Vascularized cardiac spheroids as novel 3d in vitro models to study cardiac fibrosis," *Cells Tissues Organs*, vol. 204, no. 3-4, pp. 191–198, 2017.

[131] T. C. Bracco Gartner, J. C. Deddens, E. A. Mol, M. Magin Ferrer, L. W. Van Laake, C. V. Bouten, A. Khademhosseini, P. A. Doevendans, W. J. Suyker, J. P. Sluijter *et al.*, "Anti-fibrotic effects of cardiac progenitor cells in a 3d-model of human cardiac fibrosis," *Frontiers in cardiovascular medicine*, vol. 6, p. 52, 2019.

[132] N. Sun, M. Yazawa, J. Liu, L. Han, V. Sanchez-Freire, O. J. Abilez, E. G. Navarrete, S. Hu, L. Wang, A. Lee *et al.*, "Patient-specific induced pluripotent stem cells as a model for familial dilated cardiomyopathy," *Science translational medicine*, vol. 4, no. 130, pp. 130ra47–130ra47, 2012.

[133] H. S. Hwang, D. O. Kryshtal, T. K. Feaster, V. Sánchez-Freire, J. Zhang, T. J. Kamp, C. C. Hong, J. C. Wu, and B. C. Knollmann, "Comparable calcium handling of human ipsc-derived cardiomyocytes generated by multiple laboratories," *Journal of molecular and cellular cardiology*, vol. 85, pp. 79–88, 2015.

[134] "Method of the year 2017," https://www.nature.com/articles/nmeth.4575, accessed on: 19-10-2021.

[135] W. Keung, P. K. Chan, P. C. Backeris, E. K. Lee, N. Wong, A. O. Wong, G. K. Wong, C. W. Chan, B. Fermini, K. D. Costa *et al.*, "Human cardiac ventricular-like organoid chambers and tissue strips from pluripotent stem cells as a two-tiered assay for inotropic responses," *Clinical Pharmacology & Therapeutics*, vol. 106, no. 2, pp. 402–414, 2019.

[136] M. L. Schulze, M. D. Lemoine, A. W. Fischer, K. Scherschel, R. David, K. Riecken, A. Hansen, T. Eschenhagen, and B. M. Ulmer, "Dissecting hipsc-cm pacemaker function in a cardiac organoid model," *Biomaterials*, vol. 206, pp. 133–145, 2019.

[137] R. A. Li, W. Keung, T. J. Cashman, P. C. Backeris, B. V. Johnson, E. S. Bardot, A. O. Wong, P. K. Chan, C. W. Chan, and K. D. Costa, "Bioengineering an electro-mechanically functional miniature ventricular heart chamber from human pluripotent stem cells," *Biomaterials*, vol. 163, pp. 116–127, 2018.

[138] P. Hoang, J. Wang, B. R. Conklin, K. E. Healy, and Z. Ma, "Generation of spatial-patterned early-developing cardiac organoids using human pluripotent stem cells," *Nature protocols*, vol. 13, no. 4, pp. 723–737, 2018.

[139] M. Devarasetty, S. Forsythe, T. D. Shupe, S. Soker, C. E. Bishop, A. Atala, and A. Skardal, "Optical tracking and digital quantification of beating behavior in bioengineered human cardiac organoids," *Biosensors*, vol. 7, no. 3, p. 24, 2017.

[140] Z. Ma, J. Wang, P. Loskill, N. Huebsch, S. Koo, F. L. Svedlund, N. C. Marks, E. W. Hua, C. P. Grigoropoulos, B. R. Conklin *et al.*, "Self-organizing human cardiac microchambers mediated by geometric confinement," *Nature communications*, vol. 6, no. 1, pp. 1–10, 2015.

[141] A. Shkumatov, K. Baek, and H. Kong, "Matrix rigidity-modulated cardiovascular organoid formation from embryoid bodies," *PloS one*, vol. 9, no. 4, p. e94764, 2014.

[142] R. K. Iyer, D. Odedra, L. L. Chiu, G. Vunjak-Novakovic, and M. Radisic, "Vascular endothelial growth factor secretion by nonmyocytes modulates connexin-43 levels in cardiac organoids," *Tissue Engineering Part A*, vol. 18, no. 17-18, pp. 1771–1783, 2012.

[143] L. L. Chiu, R. K. Iyer, J.-P. King, and M. Radisic, "Biphasic electrical field stimulation aids in tissue engineering of multicell-type cardiac organoids," *Tissue Engineering Part A*, vol. 17, no. 11-12, pp. 1465–1477, 2011.

Appendix

Table A.1: Summary of the different types of cardiac organoid models, along with their specifications and applications (from 2018 to 2021).

Organoid Type	Culture Methods	Cell Type	Readout	Ref.
human heart organoid (hHO) (2021)	EB formation: 10 000 hiPSCs/well in round bottom ultralow attachment 96-well plates (day −2). Plate centrifuged at 100xg for 3 min and placed in incubator (37° C, 5% CO_2). On day 0, RPMI 1640/B27 minus insulin with CHIR99021 (4 µM/well), BMP4 at 0.36 pM (1.25 ng/ml) and Activin A at 0.08 pM (1 ng/ml) for 24h. On day 2, RPMI/B27 minus insulin, containing 2 µM Wnt-C59 was added and plates incubated for 48h. On day 7, a second 2 µM CHIR99021 exposure was conducted for 1 h in RPMI1640/B27.	hiPSCs	human heart organoids (hHOs) closely mimicked human fetal cardiac development and presented cardiac-specific cell lineages. Developing human heart functionality and structural features were observed in hHOs. hHOs were used to model the effects of pregestational diabetes on cardiac development. Applying healthy and diabetic levels of glucose and insulin in the differentiation media resulted in enlarged structures compared to healthy conditions and reduction in mitochondria, dysfunctional lipid metabolism, and impaired structural organization.	[13]
Cardioid (2021)	7500 and 5000 hPSCs were seeded per well in ultra-low-attachment 96-well plates in E8+ ROCK, centrifuged at 200xg for 5 min. 24h later, aggregates were induced with FlyAB(Ins) with CHIR99021 (4 and 8 µM tested per cell line). Medium was exchanged every 2 days.	hPSCs	Cardioids presented a chamber-like structure. Mesodermal Wnt-BMP signalling pointed as regulator of cardioids' self-organization. Upon cryoinjury, significant migration of CFs towards the injury site was observed in trilineage cardioids with fibronectin deposition.	[100]
heart-forming organoid (HFO) (2021)	On day -4, 5000 cells per well were seeded in U-shaped ultralow-attachment 96-well plates in E8 medium + 10 µM ROCK, centrifuged at 300xg, 3 min 4° C and placed in the incubator (37° C, 5% CO_2) for 24h. On day -2, each aggregate was embedded in a Matrigel droplet. Differentiation was started on day 0 in embedded aggregates with RPMI 1640/B27 minus insulin supplemented with 7.5 µM CHIR99021. On day 3, 5 µM IWP2 (Wnt pathway inhibitor) was added for 48 h. From day 7, media was exchanged to RPMI 1640/B27 plus insulin.	hESCs	heart-forming organoids (HFOs) recapitulate cardiomyogenesis, presenting an inner core structure surrounded by a myocardial layer and morphological similarities to embryonic early heart and foregut anlagen. Vascular network formation was observed, staining for CD31. NKX2.5-KO HFOs recapitulated the phenotype of NKX2.5-KO mice, more specifically decreased CM adhesion and hypertrophy.	[102]
Cardiac Microtissue (2020)	For CMs: seeded on Matrigel coated plates (75μg/ml growth factor-reduced Matrigel) in E8 medium BPEL medium supplemented: - with vascular endothelial growth factor (VEGF) (for ECs); - with FGM3 (for CFs). Microtissues: 5000 cells (CMs, cardiac ECs, and CFs) seeded in V-bottomed 96-well microplates, incubated at 37° C, 5% CO_2 for 21 days with refreshed media every 3-4 days.	hiPSCs	Enhancement of structural, electrical maturation and mechanical contraction of hiPSC-CMs in microtissues; recapitulation of arrhythmogenic cardiomyopathy in microtissues using patient-derived hiPSC-CFs	[101]
human ventricular cardiac organoid chamber (hvCOC) (2019)	Matrigel, DMEM media with all additives, and Wnt inhibitor, IWR-1	hESCs	Cardioactive drug testing	[135]
hCO (2019)	Collagen+Matrigel. For cells mTeSR-1 medium and RPMI-B27 medium supplemented with BMP-4, Activin A, fibroblast growth factor (FGF)-2, CHIR99021 (no insulin) hCO: DMEM with additives, no glucose	Neonatal female mouse hESCs	Recognition of regulatory pathways in CMs proliferation, cardioprotective drug screening	[12]
cardiac organoid (CO) (2019)	RPMI and B27 media	Neonatal rat CMs, hiPSCs	hiPSC-CM EBs as a biological pacemaker	[136]
hCO (2018)	mouse ESCs: IDMD/Ham's F12 + N2, B27, pen/strep, 2mM GlutaMAX hiPSCs: Essential 8 medium + RPMI+B27 minus insulin with BMP4 and CHIR99021. On day 2, BMP4 and CHIR99021 are removed, following with a treatment with XAV939 for 48h	Mouse ESCs hiPSCs	Model for early heart development stages, namely the specification of FHF and SHF progenitors	[78]
hvCO (2018)	Matrigel, DMEM media with all the additives	hPSCs	Simplified heart pump measuring electrophysiological function and pump function in response to drugs	[137]
3D cardiac microchamber (2018)	mTeSR1 media or Essential 8 media in either hESC-qualified Matrigel, Geltrex basement membrane matrix, or Synthemax surface-coating solutions Microchambers formation in PDMS stencil using a cell micropatterning strategy with standard lithography techniques and surface grafting of PEG	hiPSCs	Approximate resemblance to an early-developed heart with distinct spatial organization and self-assembly	[138]
hCO (2018)	COR.4U medium, CMM media, fibroblasts were added as 10% of total cell number	iPSCs	Environmental toxin screening	[112]

Table A.2: Summary of the different types of cardiac organoid models, along with their specifications and applications (from 1997 to 2017).

Organoid Type	Culture Methods	Cell Type	Readout	Ref.
hCO (2017)	Agarose hydrogel molds (2% agarose) with organoid media (DMEM/F12 with glucose + 10% fetal bovine serum (FBS) + 1% non-essential amino acids) + 75 mL of cell suspension	hiPSC-CMs, CFs, human umbilical vein endothelial cells (HUVECs) and human adipose-derived stem cells (hADSCs)	Scaffold-free vascularized model of the developing myocardium, based on intramyocardial organization events of coronary vasculogenesis	[28]
hCO (2017)	Matrigel, mTeSR medium supplemented with 0.5% pen-strep, cells were passed with TrypLE in every 3/4 days	hESCs	Cryoinjury model for cardiac regeneration. Representation of immature human heart	[49]
Bioengineered CO (2017)	Hydrogel, CMM media with fibroblasts in 96- well plates	iPSCs	Tracking and quantifying beating behaviour	[139]
3D cardiac microchambers (2015)	RPMI/B27-Ins + 12 mM CHIR9902 (24h), with a treatmnent with inhibitor of Wnt production IWP-4 Microchamber formation in Matrigel-coated PEG-patterned substrate	hiPSCs	3D cardiac microchambers showing spatially organized lineage specification and beating behaviour upon geometric confinement	[140]
CO (2014)	Collagen conjugated Polyacrylamide (CCP), DMEM/F12 media with all additives	Mouse ESCs	Testing of ideal matrix characteristics during organoid formation	[141]
CO (2012)	CM/FB media for 7 days in microchannels	Neonatal rat heart cells and CFs	Importance of VEGF in connexin-43 modulation	[142]
Engineered CO (2011)	Matrigel coated microchannel, High glucose DMEM, L-glutamine, FBS, HEPES buffer, penicillin and streptomycin	Mouse ESCs	Electrical field stimulation on engineered CO	[143]
CO (1997)	Matrigel matrix + CM/FB medium containing DMEM and supplemented with glucose, L-glutamine, FBS, Penicillin, Streptomycin and HEPES Buffer	Neonatal rat	Importance of different cell types, improving organoid properties	[81]

Table A.3: Information on resources used for cell culture and assays performed.

Reagent or Resource	Source	Identifier
Chemicals, peptides and recombinant proteins		
Matrigel growth factor reduced, basement membrane matrix	Corning	356230
PBS, pH 7.4	Sigma-Aldrich	822184
EDTA	Thermo Fisher	15575020
PFA 4% in 13 PBS, pH 7.0–7.6	Santa cruz	30525-89-4
Penicillin/streptomycin	Gibco	10378016
BSA fraction V (10X)	Roche	10735086001
TrypLE select enzyme (10X)	Gibco	A12177
Trypan blue solution, 0.4%	Thermo Fisher	15250061
Triton X-100	Merck	X100-1L
Tween 20	Sigma-Aldrich	822184
E8 basal medium	Gibco	A1517001
RPMI 1640 medium + L-glutamine	Life Technologies	11875-093
DMEM no glucose	Life Technologies	11966025
B-27 supplement minus insulin (B27-insulin)	Life Technologies	A1895601
B-27 supplement plus insulin (B27+insulin)	Life Technologies	17504-044
KnockOut (KO) serum replacement	Gibco	10828010
ROCK inhibitor Y-27632	Roche	S1049
RevitaCell	Thermo Fisher	A2644501
CHIR99021	Selleckchem	S2924
Wnt-C59	Tocris Bioscience	5148
Maturation master mix		
D-Glucose (3mM)	Sigma Aldrich	G7021
L-lactate (10mM)	Sigma Aldrich	71718
Vitamine B12 (5mg/ml)	Sigma Aldrich	V6629
Biotin (0.82 mM)	Sigma Aldrich	B4639
Creatine monohydrate (5mM)	Sigma Aldrich	C3630
Taurine (2mM)	Sigma Aldrich	T0625
L-carnitine (2mM)	Sigma Aldrich	C0283
Ascorbic acid (0,5 mM)	Sigma Aldrich	A8960
NEAA (1x)	Thermo Fisher Scientific	11140
Albu-max 0,5% (w/v)	Thermo Fisher Scientific	11020021
Calcium assay reagents		
Cal520, AM	Abcam	ab171868
Pluronic® F-127	Sigma Aldrich	P2443
FluoroBrite DMEM Media	Thermo Fisher	A1896701

Reagent or Resource	Source	Identifier
Other		
Cryovials	VWR	479-6846
T75 cell culture flasks	Greiner	658170
6-well cell culture plates	Greiner	657160
6 wells low attachment plate	Corning Costar	3471
96 wells round-bottom ultralow attachment plate	Corning Costar	7007
24 well suspension plate	Corning Costar	3738
15 mL centrifuge tubes	Greiner	188280